

Searching for shell stars in LAMOST DR4 by probing the Fe II 42 multiplet lines

Stefan Hümmerich,^{1,2}★ Ernst Paunzen,³ and Klaus Bernhard^{1,2}

¹Bundesdeutsche Arbeitsgemeinschaft für Veränderliche Sterne e.V. (BAV), Munsterdamm 90, D-12169 Berlin, Germany

²American Association of Variable Star Observers (AAVSO), 49 Bay State Rd, Cambridge, MA 02138, USA

³Department of Theoretical Physics and Astrophysics, Masaryk University, Kotlářská 2, 611 37 Brno, Czech Republic

Accepted 2022 October 6; Revised: 2022 September 29; Received: 2022 September 8

ABSTRACT

Shell stars, in particular the cooler ones, often do not show conspicuous Balmer-line emission and may consequently be missed in surveys that specifically search for emission signatures in the H α line. The present work is aimed at identifying stars with shell-signatures via a search for strong Fe II multiplet 42 lines at $\lambda\lambda 4924, 5018, 5169 \text{ \AA}$ in archival LAMOST spectra. Candidates were selected by probing the Fe II (42) lines in the spectra of a sample of colour-preselected early-type stars using a modified version of the MKCLASS code and then categorised by visual inspection of their spectra. We identified 75 stars showing conspicuous shell features, 43 Am/CP1 stars, 12 Ap/CP2 stars, and three objects with composite spectra. Spectral types and equivalent width measurements of the Fe II (42) lines are presented for the sample of shell stars. Except for three objects, all shell stars appear significantly removed from the ZAMS in the colour-magnitude diagram, which is likely due to extinction by circumstellar material. We find a correlation between the equivalent width of the $\lambda 5169 \text{ \AA}$ line and the distance to the locus of the main-sequence stars (the larger the IR-excess, the stronger the $\lambda 5169 \text{ \AA}$ line) and studied the variability of the shell star sample using TESS data, identifying a very high proportion of double stars. All but 14 shell stars are new discoveries, which highlights the efficiency of the here presented novel approach to identify stars with subtle shell features. This study may be used as a blueprint for discovering these objects in massive spectral databases.

Key words: circumstellar matter – stars: chemically peculiar – stars: variables: general – techniques: spectroscopic

1 INTRODUCTION

A certain set of B, A, and, much more rarely, F stars shows spectroscopic evidence for the presence of circumstellar shells, which manifests itself in enhanced lines of Fe II and Ti II, emission, or deep and narrow absorption cores in the hydrogen Balmer lines, and, quite often, strong and peculiar Ca II K and weak Mg II $\lambda 4481 \text{ \AA}$ lines (Gray & Corbally 2009). A quite heterogeneous group of objects may exhibit some or all of these features, such as B-type and A-type shell stars, and Herbig Ae/Be stars.

B-type shell stars are generally regarded as classical Be stars seen edge-on (e.g. Porter & Rivinius 2003; Rivinius et al. 2006), with the latter being defined as non-supergiant B stars that show (or have shown at some time) emission in one or more of the Balmer lines (Jaschek et al. 1981). Several O and A emission-line stars are also included in this group of objects (Jaschek et al. 1986; Negueruela 2004; Li et al. 2018).

Classical Be and B-type shell stars are quite numerous and allow the investigation of the interplay of such diverse phenomena as, for example, mass loss, the development and dispersion of circumstellar disks or shells, and pulsation. They have therefore been in the focus of many studies in the past (Underhill & Doazan 1982; Rivinius et al. 2013; Baade et al. 2016; Labadie-Bartz et al. 2017, 2018; Bernhard

et al. 2018; Labadie-Bartz et al. 2022). Recently, the study of these objects benefited greatly from the advent of large-scale spectroscopic surveys (e.g. Chojnowski et al. 2015; Anusha et al. 2021; Zhang et al. 2022; Shridharan et al. 2021).

As has been hinted at above, the shell phenomenon also extends to later spectral types, that is, into the realm of the A- and even F-type stars (Slettebak 1982; Gray & Corbally 2009). These cooler objects, which are in the focus of the present investigation, are generally thought to represent the less massive counterparts of the classical Be and B-type shell stars (Abt & Moyd 1973; Gray & Corbally 2009; Bohlender 2016). Other physical mechanisms, however, can be responsible for the development of a circumstellar shell, such as binarity or evaporating, cometary-like bodies (Ferlet et al. 1987). Evidence for the presence of the latter is found in the distinct class of the β Pictoris shell stars, which possess protoplanetary disks and show variable and narrow absorption features in, for example, Fe II, Ti II, and the Ca II H&K lines.

Generally, the strength of the shell features encompasses a broad range. In extreme cases, they can completely overwhelm the stellar spectrum, rendering the classification of the central star impossible (Gray & Corbally 2009). At the other extremity there are objects that show no other peculiarities than slightly enhanced lines of Fe II and Ti II, as compared to the luminosity class derived from the hydrogen lines, mostly in combination with a weak $\lambda 4481 \text{ \AA}$ line. These stars

* E-mail: ernham@rz-online.de (SH)

seem to only possess weak or tenuous shells and are sometimes referred to as “proto-shell” stars (Gray & Garrison 1987).

The Fe II and Ti II lines (or, rather, the non-photospheric contributions to these lines) arise from metastable states in the extended circumstellar shells and are commonly termed “shell lines”. Of particular interest is the Fe II multiplet 42, which consists of three lines at $\lambda\lambda 4924, 5018, 5169 \text{ \AA}$. Shell stars can be readily recognized by their strongly enhanced Fe II (42) lines (Gray & Corbally 2009). This is particularly helpful for the identification of (cool) objects that do not show conspicuous Balmer-line profiles, let alone any appreciable Balmer-line emission. However, most recent surveys that target emission-line and shell stars specifically search for emission signatures in the H α line (Anusha et al. 2021; Zhang et al. 2022; Shridharan et al. 2021), and these objects will consequently be missed.

Here we present our efforts at identifying shell-signatures via a search for strong Fe II (42) lines using archival spectra from the fourth data release (DR4) of the Large Sky Area Multi-Object Fiber Spectroscopic Telescope (LAMOST) of the Chinese Academy of Science (Zhao et al. 2012; Cui et al. 2012).

2 SPECTROSCOPIC DATA AND TARGET SELECTION

This section describes the LAMOST spectral archive, the MKCLASS code, the sample selection process, and the spectral classification workflow.

2.1 The Large Sky Area Multi-Object Fiber Spectroscopic Telescope (LAMOST)

The LAMOST telescope, also referred to as the Guo Shou Jing¹ telescope, is based at Xinglong Observatory in Beijing, China (Zhao et al. 2012; Cui et al. 2012). It is a Schmidt telescope design with an effective aperture of 3.6–4.9 m and its optical axis fixed along the north-south meridian. With its ability to take 4000 spectra in a single exposure, the LAMOST telescope is specially suited to carry out large-scale spectral surveys and is currently involved in a survey of the entire available northern sky. The LAMOST low-resolution spectra, which form the basis of our study, have a spectral resolution of $R \sim 1800$, cover the wavelength range from about 3700 to 9000 \AA and are available to a limiting magnitude of $r \sim 19$ mag. The spectra are released to the public in consecutive data releases, which can be accessed via the LAMOST spectral archive.² The LAMOST archive is a prime resource for researchers, whose exploitation has been gathering pace during the recent years.

2.2 The MKCLASS code

2.2.1 General overview

The MKCLASS code was conceived and written by Richard O. Gray to classify stellar spectra on the MK system. It imitates the methodology of a human classifier and directly compares the input spectrum to a set of standard star spectra (Gray & Corbally 2014). Provided the input spectra are of sufficient signal-to-noise (S/N), the classifications derived by MKCLASS agree very well with the classifications derived by expert human classifiers (e.g. Gray & Corbally 2014; Gray

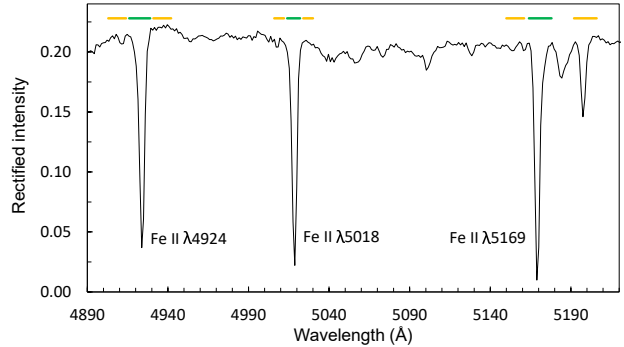


Figure 1. Graphic representation of the setup adopted to probe the Fe II (42) triplet lines at $\lambda\lambda 4924, 5018, 5169 \text{ \AA}$ in the low-resolution LAMOST spectra. Indicated are the spectral regions chosen to probe the corresponding absorption lines (green) and the neighbouring continuum flux (orange). The results were corrected for the rather prominent absorption line in the 5192–5206 \AA region.

et al. 2016; Hümmerich et al. 2018, 2020; Paunzen et al. 2021). Typical uncertainties for the derived temperature and luminosity classes amount to 0.6 and 0.5 spectral subclasses, respectively (Gray & Corbally 2014).

MKCLASS is inherently able to identify certain spectral peculiarities, such as those found, for example, in Am/CP1 stars, Ap/CP2 stars, barium stars, and carbon-rich giants. More information on the MKCLASS code is provided in Gray & Corbally (2014) and on the corresponding website.³

2.2.2 Targeting the Fe II (42) triplet lines with the MKCLASS code

We successfully employed modified versions of the MKCLASS code to search for several groups of chemically peculiar (CP) stars in spectra from LAMOST Data Release (DR) 4 (magnetic CP stars, i.e. Ap/CP2 and He peculiar stars, Hümmerich et al. 2020; HgMn/CP3 stars, Paunzen et al. 2021). To this end, the code was altered to probe additional spectral features relevant to the identification of these objects, such as certain Si II, Cr II, Sr II, and Eu II lines (Ap/CP2 stars), and Hg II and Mn II lines (HgMn/CP3 stars).

To suit the needs of the present study, the MKCLASS code was altered in a similar manner to probe the Fe II (42) triplet lines at $\lambda\lambda 4924, 5018, 5169 \text{ \AA}$ as they appear in the low-resolution LAMOST spectra ($R \sim 1800$). The corresponding flux was obtained by direct integration and then subtracted from the continuum measured in suitable adjacent spectral regions without, or with a minimum of, lines. Some experimentation was required to come up with a solution that is robust against contamination by other lines and blends in the corresponding spectral regions. As no suitable line-free neighbouring continuum region is available redwards of the $\lambda 5169 \text{ \AA}$ line, we resorted to the spectral region from $\lambda\lambda 5192 – 5206 \text{ \AA}$ and corrected for the rather prominent blend at around $\lambda 5198 \text{ \AA}$. The finally adopted solution is given in Table 1 and graphically represented in Fig. 1.

2.3 Sample selection

We initially cross-matched the complete LAMOST DR4 catalogue with the *Gaia* DR2 catalogue (Gaia Collaboration et al. 2016, 2018a;

¹ Guo Shou Jing was a Chinese astronomer, mathematician and hydraulic engineer of the Yuan Dynasty.

² <http://www.lamost.org>

³ <http://www.appstate.edu/~grayro/mkclass/>

Table 1. Spectral regions chosen to probe the Fe II (42) triplet lines at $\lambda\lambda 4924$, 5018 , 5169 Å and the neighbouring continuum flux.

(1) line	(2) continuum bluewards	(3) line region	(4) continuum redwards
$\lambda 4924$	$\lambda\lambda 4903 - 4916$	$\lambda\lambda 4916 - 4929$	$\lambda\lambda 4929 - 4942$
$\lambda 5018$	$\lambda\lambda 5006 - 5014$	$\lambda\lambda 5014 - 5022$	$\lambda\lambda 5022 - 5030$
$\lambda 5169$	$\lambda\lambda 5150 - 5164$	$\lambda\lambda 5164 - 5178$	$\lambda\lambda 5192 - 5206$

Arenou et al. 2018) and then employed a G versus $BP - RP$ diagram to select objects with $BP - RP < 0.45$ mag, with the aim of restricting the initial sample to stars hotter than a spectral type of about mid F (Hümmerich et al. 2020; Paunzen et al. 2021). As this approach is bound to miss highly reddened early-type objects or objects with bad *Gaia* photometry, we selected additional B, A and F stars via the spectral types listed in the DR4 VizieR online catalogue (Luo et al. 2018).⁴

As next step, all corresponding spectra were downloaded from the LAMOST DR4 archive, requiring a S/N of at least 50 in the Sloan g band. In the case of objects with more than one spectrum available, only the spectrum with the highest S/N was considered in the analysis.

Finally, the spectra were classified with the modified version of the MKCLASS code using the four different standard star libraries *libr18*, *libnor36*, *libsynth*, and *liblamost*, as described in Hümmerich et al. (2020). To identify spurious detections, the number of detections of the Fe II (42) triplet lines with the different standard star libraries was counted, which yielded $N_{\text{det}}(\lambda)$ for each line. As in our previous studies (Hümmerich et al. 2020 and Paunzen et al. 2021), the $N_{\text{det}}(\lambda)$ values were interpreted as an estimation of significance. Only objects were chosen that satisfied the criterion $N_{\text{det}}(\lambda 4924) > 1$ OR $N_{\text{det}}(\lambda 5018) > 1$ OR $N_{\text{det}}(\lambda 5169) > 1$, that is, we required that at least one of the Fe II (42) triplet lines was detected with at least two different libraries. The stars satisfying this criterion were assigned candidate status.

The spectra of all candidates ($N = 158$) were visually inspected to sort out artefacts and contamination by other groups of stars with prominent lines in the investigated spectral region. Spectra containing strong artefacts or other issues, such as null flux at the wavelengths of one of the Fe II (42) triplet lines, and spectra with very low S/N that entered the sample despite the selection criterion $S/N g > 50$ were sorted out ($N = 25$). The remaining sample consists of three distinct groups of stars: (i) a diverse set of stars with clearly defined Fe II (42) triplet lines of various strength ($N = 75$), (ii) a homogeneous set of stars that shows rather prominent Fe II (42) triplet lines together with a multitude of other lines and blends in the corresponding spectral region ($N = 55$), and (iii) several stars showing composite spectra that combine characteristic lines of a hot and a cool object ($N = 3$). Group (i) will be referred to in the following as the sample of shell stars, even though it contains two Herbig Ae/Be stars (cf. Section 3.1), which are not shell stars in the narrower sense of the term. Group (ii) consists of Am/CP1 ($N = 43$) and Ap/CP2 ($N = 12$) stars.

2.4 Spectral classification

Spectral types were derived using the same methodology as in our previous MKCLASS-based studies (Hümmerich et al. 2020; Paunzen et al. 2021). In a nutshell, spectral types were preferred in the order *liblamost* > *libsynth* > *libnor36* > *libr18*, except when a spectral type was derived more than once across the four spectral libraries. In that case, the most common spectral type was selected as the final classification (hereafter ‘‘MKCLASS final type’’). This procedure is exemplarily illustrated in Table 2. In the rare case of striking discrepancies between the spectral types derived with the different libraries, the best-fitting spectral type was adopted after a visual inspection of the spectra. To comply with MK standards, for the final notation, the term ‘‘shell’’ was appended to the spectral type instead of the MKCLASS output (Gray & Garrison 1987; Gray & Corbally 2009). We did not use parentheses to indicate the strength of the shell features (cf. e.g. Gray & Garrison 1987).

2.5 Equivalent widths

The equivalent widths of the Fe II (42) lines at $\lambda\lambda 4924$, 5018 , 5169 Å were measured using the program package ROBOSPEC⁵ (Waters & Hollek 2013), which is based on the assumption that all spectra are comprised of three components: the continuum level, the line solution relative to that continuum, and an error component that contains the deviation between the true spectrum and the current model. By iterating the fit of these components, it is ensured that the line and continuum solutions are not biased by each other. Prior to this process, an initial estimate of the fit parameters is constructed for each line under the assumption that the line profile is Gaussian – a good approximation for the investigated Fe II (42) lines.

As a prerequisite for using ROBOSPEC, the spectra were normalised in the corresponding spectral range using the Astropy package SPECUTILS⁶, which yields very robust results. Nevertheless, all normalised spectra were visually inspected before the calculation of the equivalent widths.

As a final step, we compared the results from ROBOSPEC for ten stars using the basic IRAF routine SPLOT. The agreement was excellent. The equivalent width measurements are included in the presentation of results in Table 6.

3 RESULTS

In this section, we present the list of shell stars identified with the specified approach, a list containing the ‘‘bycatch’’ of other astrophysically interesting objects, an investigation of the shell star sample in colour-magnitude and near-infrared colour-colour diagrams, and a photometric variability analysis.

3.1 The shell star sample

In total, we identified 75 objects with clearly defined Fe II (42) triplet lines of various strength whose spectra show shell-features of various strength (cf. Section 2.3).

In the blue-violet ($\lambda\lambda 3800 - 4600$ Å) spectral region, all stars show typical shell lines, that is, enhanced Fe II and Ti II lines, which is most readily seen in the $\lambda\lambda 4172-9$ blend due to Fe II and Ti II, the Fe II $\lambda 4233$ line, and the ‘‘forest’’ of Fe II and Ti II lines from about

⁴ <http://cdsarc.u-strasbg.fr/viz-bin/cat/V/153>

⁵ <http://www.ifa.hawaii.edu/users/watersc1/robospect/>

⁶ <https://specutils.readthedocs.io/>

Table 2. Spectral classification procedure based on the raw output of the modified MKCLASS code. Spectral types were preferred in the order *liblamost* > *libsynth* > *libnor36* > *libr18*. If common classifications exist, the most common spectral type was selected as the final classification. The columns denote: (1) LAMOST identifier. (2) MKCLASS output using the standard star libraries *libr18*, *libnor36*, *libsynth*, and *liblamost*. (3) finally adopted spectral type. The spectral types on which the final classification was based are highlighted with bold font in column (2).

(1)	(2)	(3)
LAMOST ID	Output using <i>libr18/libnor36/libsynth/liblamost</i>	SpT_final
J002559.10+555631.3	A0 II-III Fe4923 Fe5018 Fe5171 A0 II-III Fe4923 Fe5018 Fe5171 A0 II-III Fe4923 Fe5018 Fe5171 A0 III Fe4923 Fe5018 Fe5171	A0 II-III shell
J003933.02+273029.5	kA4hA9mA8 Fe4923 Fe5018 Fe5171 kA4hA8mF0 Fe5018 Fe5171 A5 III-IV Fe4923 Fe5018 Fe5171 A5 III-IV Fe4923 Fe5018 Fe5171	A5 III-IV shell
J004127.44+220716.9	kA2hA3mA6 Fe4923 Fe5018 Fe5171 A2 IV-V Fe5018 Fe5171 kA2hA4mA6 Fe4923 Fe5018 Fe5171 A2 IV-V Fe4923 Fe5018 Fe5171	A2 IV-V shell
J020138.33+561624.4	A2 IV-V Fe4923 Fe5018 Fe5171 A2 IV-V Fe4923 Fe5018 Fe5171 A3 IV-V Fe4923 Fe5018 Fe5171 A2 IV-V Fe4923 Fe5018 Fe5171	A2 IV-V shell
J020207.64+543927.9	kA1hA9mA8 Fe4923 Fe5018 Fe5171 A1 III Fe4923 Fe5018 Fe5171 kA1hA3mA6 Fe4923 Fe5018 Fe5171 A1 III-IV Fe4923 Fe5018 Fe5171	A1 III-IV shell

$\lambda 4400$ to $\lambda 4600$ Å (Gray & Corbally 2009). Figure 2 illustrates the blue-violet spectral region of four example stars. Other characteristics commonly encountered in these objects – and readily visible in this plot – are weak Mg II $\lambda\lambda 4481$ lines; peculiarly strong Ca II K lines; and rather broad lines of He I $\lambda\lambda 4026, 4144, 4387, 4471$ in the hotter stars (the upper two objects).

Figure 3 shows the corresponding region of the Fe II (42) triplet lines including the H β line ($\lambda\lambda 4800$ –5300 Å; left panel) and the region of the H α line ($\lambda\lambda 6530$ –6600 Å; right panel). All objects show strongly enhanced Fe II (42) triplet lines as well as peculiar H β profiles characterised by shell absorption cores of varying strength. The star J053918.09+361716.2⁷ is a Herbig Ae/Be star (Zhang et al. 2022).

The H α line profiles shown in the right panel of Figure 3 are equally characteristic. In particular the hotter shell stars show conspicuous emission features with a central absorption core, as seen here in all stars but the cool J200641.70+274307.0, which only shows very weak emission wings. The Herbig Ae/Be star J053918.09+361716.2 exhibits strongly asymmetric profiles in both the H β and H α lines.

The final sample of shell stars is presented in Table 6, which contains LAMOST identifiers, GAIA EDR3 coordinates, brightness measurements in the GAIA *G* band, MK spectral types, equivalent width measurements of the Fe II (42) triplet lines, and a description of the H α line profile characteristics. The notation used to describe the latter is presented in Table 3. The distribution of spectral types is shown in Fig. 4.

⁷ Unless indicated otherwise, all coordinate-based identifiers in this paper refer to LAMOST identifiers.

Table 3. Notation used to describe the H α line profile characteristics of the final sample of shell stars.

Notation	Description
0	arrow line, no emission, no absorption core, often filled-in/flat-bottomed
0(+)	conspicuously filled-in
1	narrow absorption core, emission wings absent
or very weak	
1(-)	weak absorption core
1(+)	conspicuous absorption core
2	emission wings and central absorption core
2(-)	weak emission wings
2(+)	strong emission wings
3	emission with central absorption core
4	strong emission with central absorption core
asym	asymmetric profile

All but 14 stars are new discoveries. 13 objects are contained in the list of Zhang et al. (2022), five of which are also included in the sample of Shridharan et al. (2021). One additional star (J200641.70+274307.0) is contained in the GAIA DR2-based catalogue of Vioque et al. (2020). These objects are identified by the footnotes provided after the LAMOST identifiers in Column 1 of Table 6. As LAMOST spectra have been thoroughly searched for

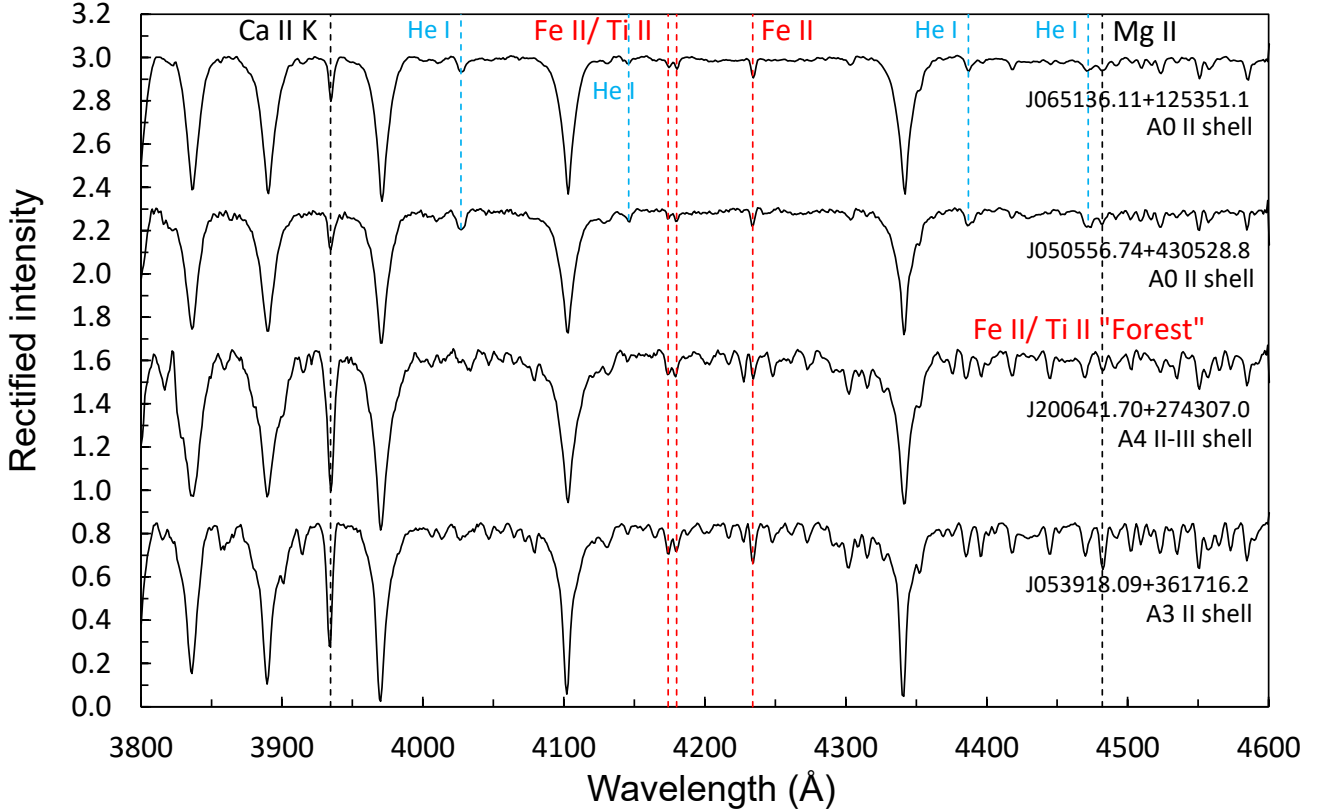


Figure 2. Blue-violet spectral region of four example spectra with shell features, based on spectra from LAMOST DR4. Some prominent lines of interest are identified.

emission-line stars (Anusha et al. 2021; Zhang et al. 2022; Shridharan et al. 2021), this is a remarkable but not unexpected result because our approach is based on a search for strong Fe II (42) lines and does not specifically target emission-line features, which may be inconspicuous or even absent in shell stars. This highlights the efficiency of the chosen approach to find shell stars in massive spectral databases.

Interestingly, two of the stars contained in the sample of Zhang et al. (2022) (J053918.09+361716.2 and J054329.26+000458.8) have been identified as Herbig Ae/Be stars. To further investigate the spectral energy distribution (SED) of these objects, we have employed the VO Sed Analyzer tool, VOSA⁸ v7.5 (Bayo et al. 2008) for fitting the available photometry. In Fig. 5 we show the SED of the two Herbig Ae/Be stars, which clearly exhibit an IR-excess redwards of $1\mu\text{m}$, which is typical for a circumstellar disk (Meeus et al. 1998).

3.2 Other astrophysically interesting objects

Apart from the shell stars, our sample also contains 55 stars with prominent Fe II (42) triplet features and a multitude of other lines and blends in the corresponding spectral region. A careful study of the corresponding spectra revealed that this group mostly consists of CP1 and CP2 stars. The CP1 stars exhibit significant underabundances of Ca and Sc and a general enhancement of the ironpeak and heavier

elements in the stellar photosphere. The CP2 stars, on the other hand, are characterised by significant overabundances of selected elements such as Si, Sr, Eu, or the rare-earth elements. Both types of star show characteristic ‘forests’ of lines in the region of the Fe II (42) triplet. Their detection by the modified MKCLASS code, therefore, does not come as a surprise.

Example spectra of a late A-type CP1 and a late A-type CP2 star in comparison to the A7 V standard star from the *liblamost* library (Hümmerich et al. 2020) are shown in Fig. 6. Both CP stars have characteristically weak Ca II K lines. While the CP1 star shows a general overabundance of the heavy elements, there is a strong selective enhancement of Sr, Cr, and Eu features in the CP2 star. This is particularly visible in the strong $\lambda 4077\text{ Å}$ blend, which contains contributions from Si II $\lambda 4076$, Cr II $\lambda 4077$, and Sr II $\lambda 4077$; the $\lambda 4130\text{ Å}$ blend, which contains contributions from Si II $\lambda\lambda 4128-30$ and Eu II $\lambda\lambda 4130$; the Cr II $\lambda 4172\text{ Å}$ line; the Eu II $\lambda 4205\text{ Å}$ line; and the Sr II $\lambda 4216\text{ Å}$ (Gray & Corbally 2009).⁹

Table 7 contains elementary data for the CP1 and CP2 stars as well as the stars showing composite spectra. We also cross-matched this subsample with LAMOST-based catalogues of CP1 and CP2 stars (Renson & Manfroid 2009; Scholz et al. 2019; Qin et al. 2019; Hümmerich et al. 2020; Shang et al. 2022), the results of which are

⁸ <http://svo2.cab.inta-csic.es/theory/vosa/>

⁹ Cf. also the Atlas of LAMOST Low-Resolution Spectra of Chemically Peculiar Stars by one of the authors (SH), which is available at http://www.appstate.edu/~grayro/mkclass/LAMOST_CP_Atlas_v1.pdf

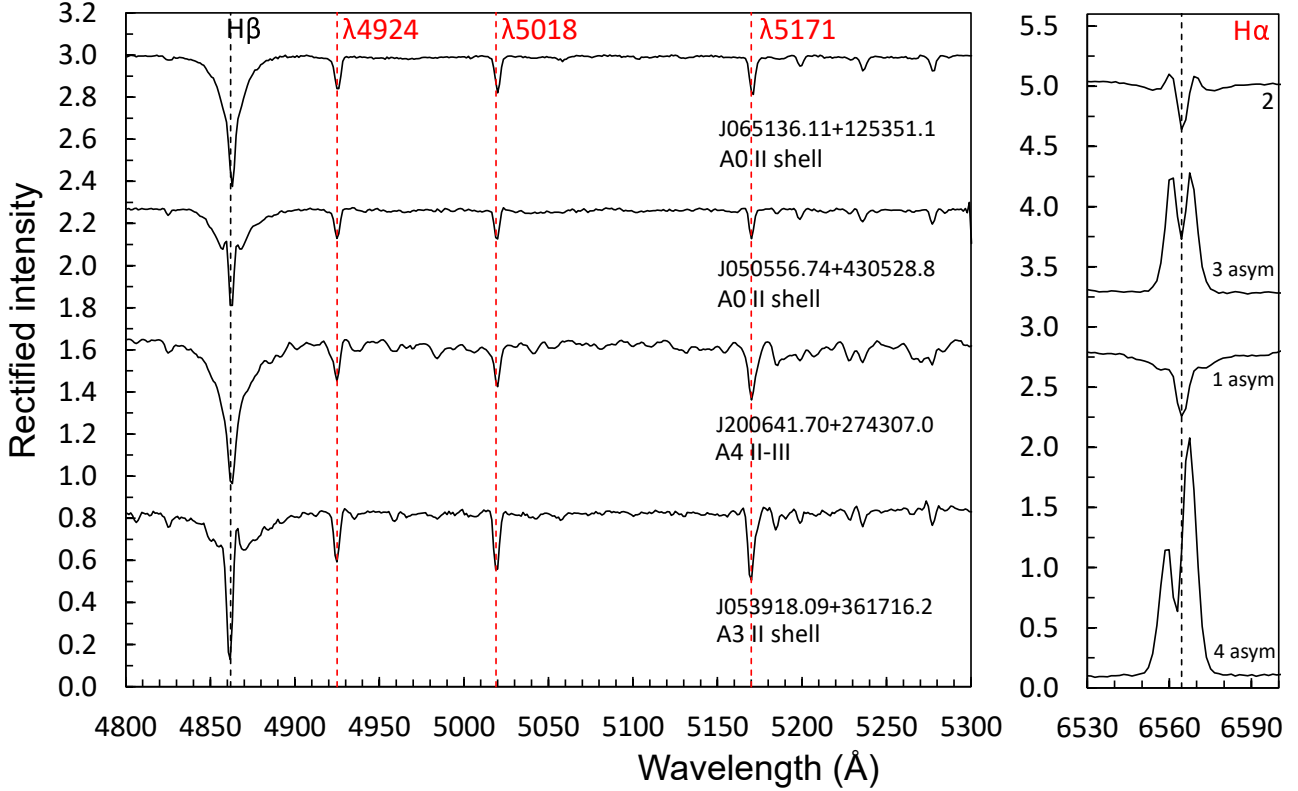


Figure 3. Spectral region of the Fe II (42) triplet lines including the H β line (left panel) and the corresponding region of the H α line (right panel), based on spectra from LAMOST DR4. Some prominent lines of interest are identified. The objects are the same as shown in Fig. 2. The numbers next to the H α line profiles correspond to the notation used to describe the H α line profile characteristics (cf. Table 3).

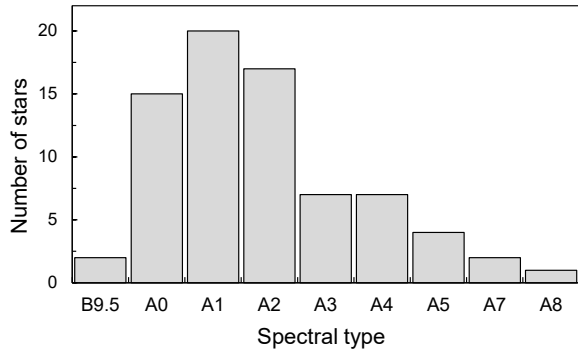


Figure 4. Distribution of spectral types among the sample of shell stars.

included in Column 9 of Table 7. It is noteworthy that almost all the CP stars have been identified correctly in former studies.

3.3 Astrophysical parameters, equivalent widths, binarity, and IR-excess of the shell star sample

We constructed the colour-magnitude diagram (CMD) for the final sample of shell stars using the homogeneous *Gaia* DR2 photometry from Arenou et al. (2018). The interstellar reddening (absorption) needs to be taken into account because most of our sample stars are members of the Galactic disk and situated beyond 500 pc from

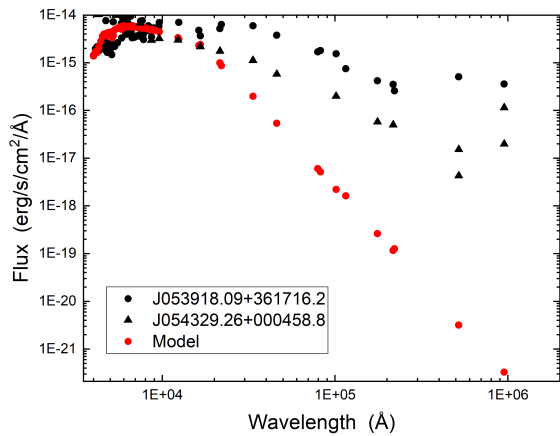


Figure 5. IR excesses for the Herbig Ae/Be stars J053918.09+361716.2 and J054329.26+000458.8, which are typical for a circumstellar disk.

the Sun. Unfortunately, Strömgren-Crawford indices, which allow a reliable reddening estimation, are not available (Paunzen 2015). We therefore relied on the three-dimensional reddening map of Green et al. (2019). For the distances, we used the values published by Bailer-Jones et al. (2018) who applied a weak distance prior that varies smoothly as a function of Galactic longitude and latitude according to a Galaxy model. The estimated extinctions were then

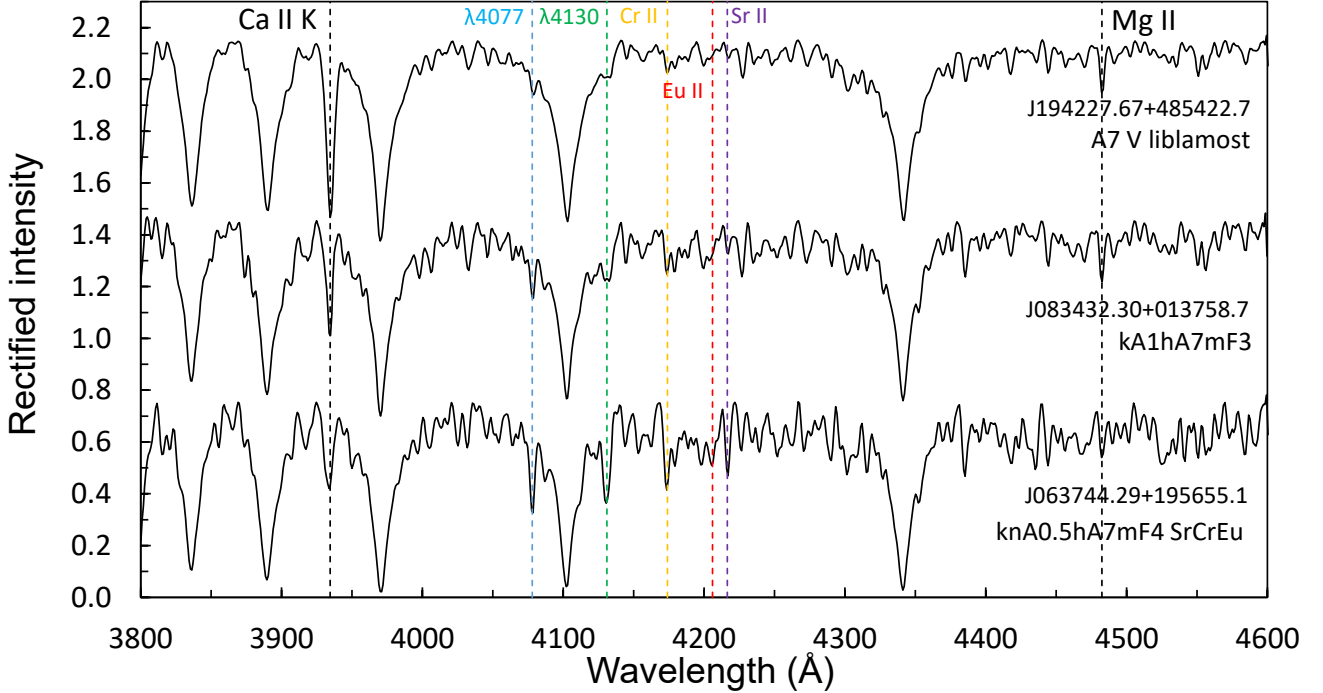


Figure 6. Blue-violet spectral region of, from top to bottom, the A7 V standard star from the *liblamost* library, an example CP1/Am star, and an example CP2/Ap star, based on spectra from LAMOST DR4. Some prominent lines of interest are identified.

transformed to the *Gaia* photometric systems using the coefficients listed in [Gaia Collaboration et al. \(2018b\)](#). The distances were directly converted into the absolute magnitudes $M(G)$.

In Fig. 7, we present the $M(G)_0$ versus $(BP - RP)_0$ diagram together with the main-sequence PARSEC isochrones ([Bressan et al. 2012](#)) for a solar metallicity of $[Z] = 0.0152$. The Herbig Ae/Be stars J053918.09+361716.2 and J054329.26+000458.8 (see Section 3.1) are clearly separated from the other objects. Besides three stars, all objects are located quite far away from the zero-age main sequence (ZAMS). This is not expected because they should cover the whole area up to the ZAMS ([Jaschek et al. 1988](#)). This discrepancy can be explained by “the missing” extinction due to the circumstellar material. In our analysis, we have only corrected for the interstellar absorption. An additional 0.5 mag in V would bring most of the stars very close to the ZAMS (see Fig. 7). Without knowledge about the strength of this additional contribution, it does not make sense to further calibrate any astrophysical parameters. Only fitting the hydrogen lines and, to some extent, the SED could further narrow down the effective temperature range for the individual stars.

To further investigate the IR-excess of the shell star sample, we performed a cross-match with the JHK_S 2MASS survey ([Skrutskie et al. 2006](#)). We then constructed a $(J - H)_0$ versus $(H - K_S)_0$ diagram using the corresponding absorption coefficients from [Yuan et al. \(2013\)](#). We note that the reddening is smaller than in the optical region, therefore the above mentioned effect is not so severe. The result is plotted in Fig. 8, in which two distinct groups separated at $(J - H)_0 = 0.2$ mag are visible. The reddening vector ([Bessell & Brett 1988](#)) points toward the line of the normal type main-sequence stars. To shift the stars of the second group close to the main sequence, correcting for an absorption of two to three magnitudes in V is necessary. Such high values are very unlikely taking into account

the derived spectral types and the corresponding shift in the CMD (Figure 7).

There is a correlation of the $(J - H)_0$ colour with $\text{EQW}_{\lambda 5169}$, whereas the other two lines do not show a correlation (Table 4). Figure 8 illustrates that stars which are more distant to the standard line tend to have larger equivalent widths, that means the larger the IR-excess, the stronger the $\lambda 5169 \text{ \AA}$ line. A similar effect can be seen in the CMD (Fig. 7). Objects closer to the ZAMS tend to have weaker $\lambda 5169 \text{ \AA}$ lines.

As described in Section 2.5, we measured the equivalent widths of the Fe II (42) triplet lines of the shell star sample (Table 6). For the calculation of the correlations between the corresponding equivalent widths, we use the R^2 value (Table 4) which is a measure of the goodness of fit. As expected, the three equivalent widths are correlated, with $\text{EQW}_{\lambda 4924}$ versus $\text{EQW}_{\lambda 5169}$ showing the weakest, but still statistically significant, correlation (Figure 9). This can be interpreted as an indication that these two lines are formed in different stellar environments/regions ([Eiroa et al. 2021](#)). Although the here employed LAMOST spectra have only classification resolution ($R \sim 1800$), our results prove that they can be used in future efforts to model the environments of shell stars in more detail ([Miroshnichenko et al. 1996](#)).

Finally, we checked the *Gaia* DR2 and DR3 for indications of binarity among the shell star sample. To this end, we used the “Dup” flag and the RUWE parameter, which are good indicators ([Zavada & Přška 2022](#)). In Table 5, we list the corresponding indicators for the stars that show conspicuous values (RUWE > 1.6 was adopted as threshold). Six of these stars have been identified as eclipsing binaries (J032704.99+434028.5, J040713.90+291832.1, J074455.91+042805.1, J075535.94-

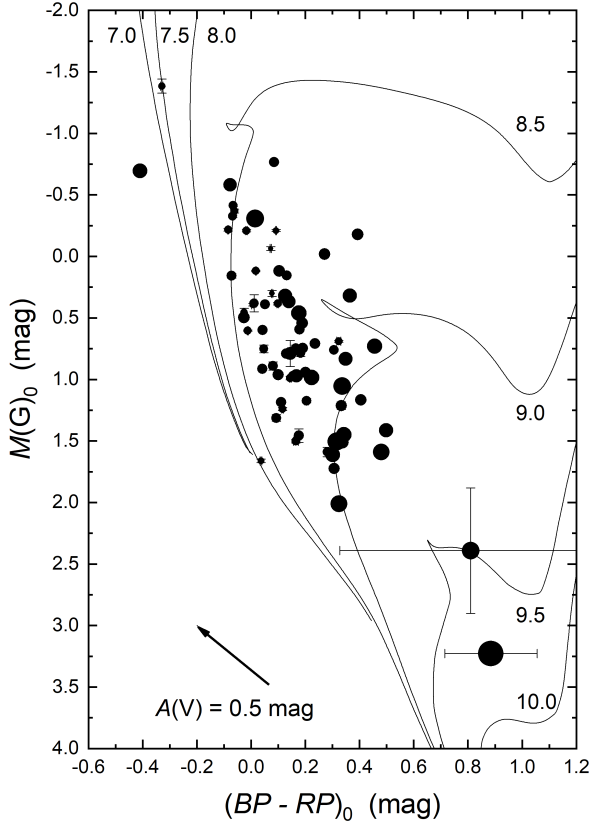


Figure 7. The CMD for our target star sample together with main-sequence PARSEC isochrones (Bressan et al. 2012) for a solar metallicity of $[Z] = 0.0152$. The symbol sizes are proportional to equivalent widths of the Fe II (42) line at $\lambda\lambda 5169 \text{ \AA}$ (Table 6). Also shown is the reddening vector for $A(V) = 0.5 \text{ mag}$.

Table 4. R^2 values as a measure of the goodness of fit for the linear regression between the tabulated parameters. The two outlying datapoints of the Herbig Ae/Be stars J053918.09+361716.2 and J054329.26+000458.8 were excluded from the statistical analysis.

	EQW _{λ4924}	EQW _{λ5018}	EQW _{λ5169}
EQW _{λ4924}		0.7058	0.3149
EQW _{λ5018}			0.6574
$(J - H)_0$	0.0025	0.0216	0.3012

033455.4, J092110.64+283147.9) or ellipsoidal variables (J232258.57+541829.2; cf. also Table 8).

3.4 Variability analysis

The Transiting Exoplanet Survey Satellite (TESS) aims at the discovery of transiting exoplanets (Ricker et al. 2014, 2015; Campante et al. 2016).¹⁰ To this end, four cameras (effective aperture size 10 cm) equipped with f/1.4 lenses and MIT/Lincoln Lab CCD detectors (4096x4096 pixels; imaging area of 2048x2048 pixels; remain-

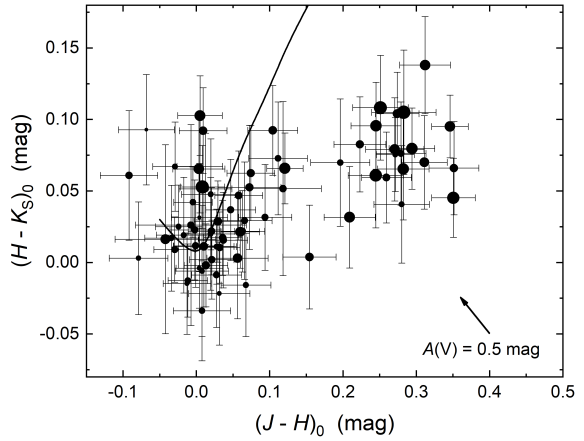


Figure 8. The $(J - H)_0$ versus $(H - K_s)_0$ diagram showing two groups of objects. The line represents the locus of the normal type main sequence stars (Bessell & Brett 1988). The symbol sizes are proportional to equivalent widths of the Fe II (42) line at $\lambda\lambda 5169 \text{ \AA}$ (Table 6). The two outliers J053918.09+361716.2 and J054329.26+000458.8 were omitted.

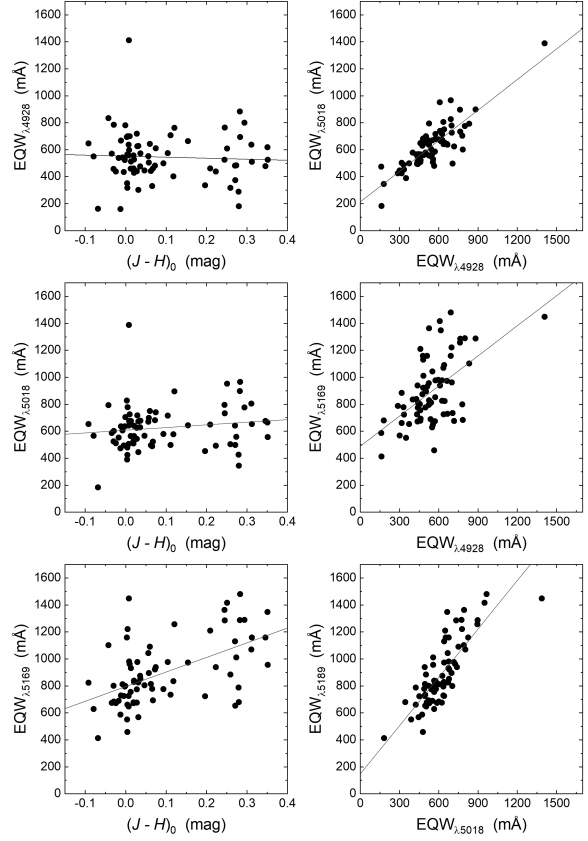


Figure 9. The correlations of the $(J - H)_0$ magnitudes with the different equivalent widths (left columns) and the equivalent widths among themselves (right columns). The R^2 values of the individual fits are listed in Table 4.

¹⁰ <https://heasarc.gsfc.nasa.gov/docs/tess/>

Table 5. Binarity indicators from *Gaia* DR2 and DR3.

ID_LAMOST	RUWE	Dup(DR3)	Dup(DR2)	ID_LAMOST	RUWE	Dup(DR3)	Dup(DR2)
J002559.10+555631.3	0.951	0	1	J054358.96+491845.6	0.954	1	1
J020138.33+561624.4	0.998	0	1	J054834.63+234141.4	1.120	1	1
J020207.64+543927.9	1.919	0	0	J064230.24+092626.7	0.845	1	1
J020820.76+562433.0	0.952	0	1	J074455.91+042805.1	1.078	1	1
J032704.99+434028.5	0.965	1	1	J075535.94–033455.4	1.405	0	1
J033909.14+523714.5	0.931	0	1	J092110.64+283147.9	3.920	0	0
J035033.65+525943.2	1.906	0	1	J180605.37+020543.8	1.843	0	0
J040713.90+291832.1	1.592	1	1	J195131.48+484558.9	4.257	0	0
J041308.41+534045.9	0.922	1	1	J200641.70+274307.0	1.157	0	1
J053235.07+495218.6	1.838	0	0	J231357.71+545812.0	0.903	1	1
J054329.26+000458.8	2.059	0	0	J232258.57+541829.2	1.033	0	1

ing pixels used as frame-store for rapid shutterless readout) are used, which produce single-passband (6000–10000 Å) light curves. TESS data have a cadence of 30 minutes and 2 minutes for the summed full-frame images and the “postage stamp” observations centered on 20000 preselected stars. With their wealth of high-cadence high-precision time-series data, the TESS archives are an excellent starting point for stellar variability studies.

The full-frame TESS images have been processed by Huang et al. (2020a,b) and Kunimoto et al. (2021) to provide quick-look pipeline light curves. Data from all available sectors (up to sector 35) for the final shell star sample were downloaded via MAST¹¹ and included in the analysis. In total, data from 72 sectors could be retrieved for 48 stars.

After a visual inspection of all light curves and the removal of apparent outliers, a period analysis of the uncorrected SAP flux data was performed using the Lomb-Scargle method as implemented in the software package PERANSO (Paunzen & Vanmunster 2016).

Significant periods as well as preliminary types are given in Table 8, which also lists periods and types from the International Variable Star Index (VSX; Watson et al. 2006) of the American Association of Variable Star Observers (AAVSO). Due to the limited observation time in a TESS sector (~27d on average), only periods of a maximum of 14 d could be reliably recorded.

In addition to a few objects with irregular variability ($N = 3$) and presumed pulsators ($N = 3$), there is a high number of eclipsers and presumably ellipsoidal variables ($N = 18$) among the stars of our final sample. This indicates a very high proportion of double stars among the shell star sample, which is not surprising, as binarity can be responsible for the development of a circumstellar shell (Ferlet et al. 1987).

The JD light curves of all variables among the final sample of shell stars are provided in the Appendix (Section A).

4 CONCLUSIONS

We carried out a search for shell stars by targeting the Fe II (42) lines at $\lambda\lambda 4924, 5018, 5169$ Å in LAMOST DR4 spectra with a modified version of the MKCLASS code. This led to the identification of three distinct groups of stars. 75 stars show shell features, that is, enhanced Fe II and Ti II lines as well as typical H α profiles such as emission features, a central absorption core, and/or filled-in line cores, in agreement with a shell star classification. Two of these

stars (J053918.09+361716.2 and J054329.26+000458.8) are Herbig Ae/Be stars (Zhang et al. 2022). Apart from that, we identified 43 Am/CP1 stars, 12 Ap/CP2 stars, as well as three stars showing composite spectra with lines indicative of a hot and a cool object.

We present MK class spectral types and equivalent width measurements of the Fe II (42) lines for the sample of shell stars, which was also investigated in the $M(G)_0$ vs. $(BP - RP)_0$ and $(J - H)_0$ vs. $(H - K_S)_0$ parameter spaces. Except for three objects, all stars appear significantly (~ 0.5 mag in V) removed from the ZAMS in the CMD, which is likely due to extinction caused by circumstellar material. This assumption is further corroborated by the results from the near-infrared colour-colour diagram, which shows two distinct groups of stars separated at $(J - H)_0 = 0.2$ mag. As expected, the Herbig Ae/Be stars are clearly separated from the other objects in both parameter spaces.

We find a correlation between the position of a star in both diagrams and the equivalent width of the $\lambda 5169$ Å line, in the sense that the further a star is removed from the locus of the main-sequence stars, the larger is $EQW_{\lambda 5169}$. Put differently, the larger the IR-excess, the stronger is the $\lambda 5169$ Å line. The strongest correlation was found between $(J - H)_0$ and $EQW_{\lambda 5169}$. We find evidence that the $\lambda 4924$ Å and $\lambda 5169$ Å lines are formed in different stellar environments/regions and show that the low-resolution LAMOST spectra are generally suited for modeling the environments of shell stars in more detail.

Using TESS data, we investigated the photometric variability of the shell stars. With 18 eclipsers and ellipsoidal variables, we find a very high proportion of double stars. Likely, binarity is responsible for the development of the circumstellar shell in these objects.

All but 14 shell stars are new discoveries, which highlights the efficiency of the chosen approach to identify objects with subtle shell features that, for the most part, do not show strong Balmer-line emission and will consequently be missed in surveys that specifically search for emission signatures in the H α line. Therefore, by opening up a new way of identification, our study adds a further piece to the puzzle of understanding the various manifestations of the shell star phenomenon and may be used as a blueprint for discovering these objects in massive spectral databases.

5 DATA AVAILABILITY

The data underlying this article are available in the article and in its online supplementary material.

¹¹ <https://archive.stsci.edu/hlsp/qlp>

Table 6. Essential data for our sample stars, sorted by increasing right ascension. The columns denote: (1) LAMOST identifier. (2) LAMOST observation ID. (3) Alternativ identifier. (4) Right ascension (J2000; GAIA EDR3). (5) Declination (J2000; GAIA EDR3). (6) G mag (GAIA EDR3). (7) Spectral type. (8) Sloan g band S/N ratio of the analysed spectrum. (9) Equivalent width (mÅ) of the $\lambda 4924$ Å line. (10) σ EQW (mÅ). (11) Equivalent width (mÅ) of the $\lambda 5018$ Å line. (12) σ EQW (mÅ). (13) Equivalent width (mÅ) of the $\lambda 5169$ Å line. (14) σ EQW (mÅ). (15) H α line profile characteristics.

(1) ID_LAMOST	(2) ObsID	(3) ID_alt	(4) RA(J2000)	(5) Dec(J2000)	(6) G mag	(7) SpT_final	(8) S/N _g	(9) EQW _{λ4924}	(10) σ EQW	(11) EQW _{λ5018}	(12) σ EQW	(13) EQW _{λ5169}	(14) σ EQW	(15) H α
J002559.10+555631.3	171103150	GSC 03657-00187	00 25 59.097	+55 56 31.114	11.999	A0 II-III shell	178.2	570.4	2.9	586.0	0.0	673.1	0.1	2
J003933.02+273029.5	157503180	GSC 01744-02329	00 39 33.025	+27 30 29.417	12.503	A5 III-IV shell	154.8	616.8	0.6	663.9	0.3	1347.0	1.3	2(-)
J004127.44+20716.9 ^{3a}	194501119	GSC 01193-00234	00 41 27.442	+20 07 16.944	11.712	A2 IV-V shell	230.1	483.3	0.9	558.1	0.5	1011.0	0.8	2(+)
J021038.33+561624.4	380711095	UCAC4 732-019419	02 01 38.341	+56 16 24.493	14.307	A2 IV-V shell	119.5	481.4	0.5	681.1	0.5	922.4	0.4	1(-)
J02207.64+543927.9	380804167	GSC 03689-00919	02 02 07.642	+54 39 28.010	11.422	A1 III-IV shell	419.1	573.1	1.2	678.2	0.3	851.9	0.1	1 asym
J020820.76+562433.0	380812126	HD 12921	02 08 20.633	+56 24 35.290	10.119	A0 III-IV shell	445.7	538.6	0.9	551.6	0.0	689.3	0.1	1 asym
J032040.87+52334.6 ^{2-3a}	253614211	GSC 03322-00936	03 02 40.875	+52 23 34.692	12.112	A1 II shell	103.1	1410.0	0.1	1388.0	0.0	1448.0	0.1	4 asym
J031003.35+551804.4	244009232	HD 232754	03 10 03.359	+55 18 01.367	9.564	A2 III-IV shell	570.6	541.6	0.9	605.1	0.0	812.4	0.1	1(-) asym
J031638.78+494256.2	393114190	GSC 03319-00602	03 16 38.777	+49 42 55.989	11.106	A2 IV-V shell	279.9	512.1	0.3	674.7	0.0	930.6	0.3	1(-)
J031841.75+462842.1	408714242	GSC 03311-01885	03 18 41.776	+46 28 40.974	10.913	A2 IV shell	134.8	476.2	0.2	628.6	0.1	873.3	0.2	0
J031909.14+192811.7	387704144	BD+18 457	03 19 08.931	+19 28 11.753	9.537	A5 III shell	503.0	642.0	0.2	750.0	0.1	1090.0	0.4	0
J032074.99+434028.5	96515069	GSC 02873-01933	03 27 04.997	+43 40 28.556	10.181	A4 IV-V shell	304.2	480.6	0.4	641.9	1.2	1129.0	0.5	2
J033999.14+523714.5	374616043	GSC 03716-00037	03 39 09.142	+52 37 14.550	12.146	A0 II-III shell	152.7	557.9	1.3	528.2	0.5	672.0	0.1	2(-)
J034636.05+441159.3	185201110	GSC 02875-01237	03 46 36.054	+44 11 59.403	11.520	A1 IV shell	237.3	523.6	1.7	635.7	0.0	795.1	0.1	0(+) asym
J035000.80+580406.0	157904161	GSC 03725-01226	03 50 00.807	+58 04 06.118	11.470	A1 II-III shell	230.0	350.8	0.6	389.4	0.4	550.9	0.1	1(-) asym
J035033.65+525943.2	374611112	GSC 03717-00421	03 50 33.658	+52 59 43.279	13.000	A7 III-IV shell	110.2	551.6	1.4	669.5	0.2	1043.0	1.1	0
J035205.73+351059.1	181504205	GSC 02364-02043	03 52 50.733	+35 10 59.126	14.084	A3 III-IV shell	152.2	330.7	0.4	488.6	0.1	777.6	0.4	0(+) asym
J040713.90+291832.1	370010068	GSC 01826-00710	04 07 13.878	+29 18 32.426	11.397	A2 IV shell	369.8	524.1	0.3	556.7	0.2	955.2	0.7	1
J041308.81+543045.9	351401884	GSC 03718-00545	04 13 08.415	+54 30 45.956	12.785	A2 III shell	115.4	497.8	0.3	578.8	0.1	775.9	0.3	1(-) asym
J041638.47+530600.9 ^{3a}	169203247	GSC 03719-00690	04 16 38.473	+53 06 00.846	12.139	A0 II shell	138.5	718.3	1.2	624.1	0.5	675.2	0.1	3
J043336.04+51232.6 ^{2-3a}	275204156	GSC 03324-00138	04 33 36.042	+45 12 32.709	11.803	A0 Ib-II shell	133.3	783.5	0.2	601.3	0.1	683.5	0.2	3
J043415.66+405139.5	295303158	UCAC4 655-02246	04 34 15.666	+40 51 39.552	14.088	A1 III shell	121.9	439.5	1.0	543.3	0.1	773.1	0.2	1
J043948.40+474848.5	217903222	GSC 03346-00854	04 39 48.401	+47 48 48.587	11.051	A4 III shell	247.8	662.9	1.3	642.3	0.1	972.4	0.6	1
J044307.81+571907.8	409716058	GSC 03741-00200	04 43 07.813	+57 19 07.806	12.550	A1 III shell	119.3	373.1	0.7	497.5	0.2	652.9	0.1	1(-) asym
J050435.48+402559.7 ^{3a}	315109045	UCAC4 653-028138	05 04 35.489	+40 25 59.682	14.133	A1 II shell	129.3	556.1	1.2	505.3	0.5	646.4	0.2	2(+) asym
J050556.74+430528.8 ^{2-3a}	36496120	GSC 02903-00983	05 05 56.760	+43 05 28.871	13.310	A0 II shell	124.4	564.8	1.4	479.2	0.6	457.1	0.1	3 asym
J051428.45+274243.4	15502153	GSC 01854-00033	05 14 28.465	+27 43 24.555	11.595	A2 III-IV shell	141.4	798.9	1.3	775.1	1.1	1289.0	0.9	2(-)
J053235.07+495218.6	190911156	GSC 03367-01174	05 32 35.073	+49 52 18.684	11.361	A1 III-IV shell	162.1	434.2	0.9	493.7	0.0	724.6	0.2	1(-) asym
J053414.62+215213.6	195010034	GSC 01309-01353	05 34 14.626	+21 52 13.641	11.387	A4 III shell	231.0	442.2	0.3	495.1	0.2	814.4	0.3	0 asym
J053918.09+361716.7 ^{2-3b}	380515103	GSC 02416-00657	05 39 18.088	+36 17 16.214	14.710	A3 II shell	137.2	936.5	1.4	1080.0	0.1	1426.0	0.3	4 asym
J054113.82+351910.7 ^a	297004149	GSC 02412-01090	05 41 13.827	+35 19 10.725	11.020	B9.5 III shell	268.0	780.0	1.0	703.6	0.0	799.2	0.1	3 asym
J054239.89+174652.7	393313172	HD 246608	05 42 39.841	+17 46 53.528	10.920	A1 III shell	395.1	526.6	1.3	639.4	0.4	828.5	0.3	1
J054329.26+000458.8 ^{2-3b}	326912175	HD 290828	05 43 29.252	+00 04 58.970	11.676	A7 Ib-II shell	115.7	1164.0	1.0	1448.0	0.4	2064.0	1.4	4 asym
J054358.96+491845.6	191012008	GSC 03368-01318	05 43 58.958	+49 18 45.706	11.424	A8 II shell	112.9	762.4	1.8	895.4	0.4	1257.0	0.9	0(+) asym
J054834.63+324141.4	116210055	BD+23 1058	05 48 34.637	+23 41 41.489	10.921	A1 III-IV shell	171.8	300.8	0.3	445.2	0.1	567.7	0.2	0(+) asym
J055140.83+414108.5	124303201	GSC 02920-02782	05 51 40.835	+41 41 08.500	12.615	A0 III shell	65.8	162.3	6.3	183.1	5.9	413.0	3.5	0
J055340.45+332003.9	269313053	UCAC4 617-029482	05 53 40.456	+33 20 03.995	14.269	A3 III-IV shell	105.6	706.8	0.8	496.5	0.8	734.3	0.3	0 asym
J055441.84+223317.7	434407220	GSC 01863-02412	05 54 41.850	+22 33 17.763	11.185	A3 III shell	130.1	596.3	1.3	676.3	0.1	979.7	0.4	0 asym
J055907.94-060737.6 ^{3a}	211510003	GSC 04781-00953	05 59 07.949	-06 07 37.675	12.108	A3 IV shell	127.9	509.9	3.8	653.5	1.3	1158.0	1.3	2(+) asym
J060706.46+424554.7	165716036	UCAC4 575-024208	06 07 06.470	+45 25 47.138	13.847	A0 II shell	61.4	459.0	1.4	564.3	0.1	755.4	0.2	2
J061810.01+411332.0	378007213	GSC 02930-00867	06 18 10.012	+41 13 32.113	11.615	A3 III shell	268.1	693.1	0.1	825.9	0.1	1158.0	0.4	1
J062416.04+422125.4	378006164	GSC 02935-01774	06 24 16.047	+42 21 25.477	11.073	A4 IV shell	304.3	478.3	1.1	675.9	0.7	1158.0	0.5	1
J062616.73+174526.9	435515074	HD 257117	06 26 18.745	+17 45 27.254	11.345	A2 IV shell	427.0	625.1	2.9	716.2	0.0	976.0	0.2	0
J062724.55+234913.0	201604230	UCAC4 570-028755	06 27 24.551	+23 49 31.048	15.252	A2 IV shell	105.8	401.0	0.3	577.0	0.2	833.9	0.2	1(-) asym
J064142.55+031421.9	385412092	GSC 00151-01200	06 41 42.552	+03 14 21.954	13.017	A1 III shell	106.6	610.1	0.1	739.4	0.0	938.6	0.2	1
J064230.24+092626.7	37103019	HD 262371	06 42 30.247	+09 26 26.726	9.922	A0 III shell	338.4	438.6	0.5	509.8	0.0	671.3	0.1	0
J064751.97+522321.9	264709144	GSC 03402-01356	06 47 51.974	+52 23 21.876	12.838	A5 IV-V shell	108.6	525.6	2.0	794.4	0.4	1363.0	0.6	0(+) asym
J065136.11+125351.1 ^{3a}	38714083	HD 265136	06 51 36.153	+12 53 51.562	10.277	A0 II shell	312.1	667.3	1.0	636.3	0.4	729.2	0.0	2
J065141.20+070357.7	34803143	HD 265284	06 51 41.202	+07 03 57.750	10.883	A3 II-III shell	215.9	444.5	0.2	566.5	0.1	804.8	0.3	0
J065300.06+010730.6	368901030	GSC 00149-01072	06 53 00.062	+01 07 30.643	12.472	A3 II-III shell	105.5	574.7	0.1	715.6	0.1	975.9	0.5	0
J065606.26+033757.5	368904202	GSC 00153-01723	06 56 06.264	+03 37 57.524	13.402	A1 III shell	100.6	461.0	1.8	521.7	0.1	692.8	0.3	1
J070219.92+162845.4	84409116	GSC 01344-00359	07 02 19.921	+16 28 45.453	13.394	A2 IV shell	50.3	181.2	1.6	344.6	0.6	678.7	2.0	0(+) asym
J071200.59+241137.2	177916248	GSC 01896-00475	07 12 00.593	+24 11 37.376	12.633	A1 IV shell	150.8	316.4	1.6	424.2	0.1	659.3	0.3	0(+) asym
J071340.29+380623.9 ^{3a}	184912129	HD 55200	07 13 40.582	+38 06 30.260	8.347	A0 II-III shell	443.6	832.6	0.7	792.7	0.0	1102.0	0.5	2(+) asym
J071630.57+053405.5	369602069	GSC 00172-00143	07 16 30.576	+05 34 05.521	11.043	A1 III shell	441.4	460.4	0.6	508.1	0.0	677.9	0.1	1
J072719.01+015251.6	88611215	GSC 00169-00831	07 27 19.013	+01 52 51.702	11.286	A2 III shell	149.4	427.6	0.3	564.5	0.1	837.8	0.5	0 asym
J074455.91+042805.1	263916013	GSC 00187-												

Table 7. Essential data for the CP1 and CP2 stars and the stars with composite spectra, sorted by increasing right ascension. The columns denote: (1) LAMOST identifier. (2) LAMOST observation ID. (3) Alternative identifier. (4) Right ascension (J2000; GAIA EDR3). (5) Declination (J2000; GAIA EDR3). (6) G mag (GAIA EDR3). (7) Sloan g band S/N ratio of the analyzed spectrum. (8) Type. (9) References.

(1) ID_LAMOST	(2) ObsID	(3) ID_alt	(4) RA(J2000)	(5) Dec(J2000)	(6) G mag	(7) S/N g	(8) Type	(9) Ref
J010651.35+154426.9	409510074	HD 6590	01 06 51.168	+15 44 26.921	9.998	416.0	CP2	1,2,4
J031043.71+480727.8	263604028	GSC 03314-01599	03 10 43.717	+48 07 27.866	12.714	160.4	CP2	2,4
J045926.29+535030.4	377907100	GSC 03734-01043	04 59 26.172	+53 50 30.516	10.918	291.8	CP2	2,4
J052739.41+533935.4	425715081	GSC 03748-01827	05 27 39.457	+53 39 35.696	16.891	385.1	CP2	2,4
J054547.46+400703.6	286206027	GSC 02915-01913	05 45 47.464	+40 07 03.687	11.925	191.9	CP2	2,4
J060259.74+290339.2	3109241	UCAC4 596-027865	06 02 59.747	+29 03 39.287	14.446	24.0	CP2	
J063114.53+184730.7	435511229	HD 258682	06 31 14.464	+18 47 31.872	10.752	187.4	CP2	2,4
J063744.29+195655.1	431606168	HD 47103	06 37 44.072	+19 56 55.155	9.176	811.4	CP2	1,2,3,4,5
J065216.71+205412.6	410003112	GSC 01343-00132	06 52 16.711	+20 54 12.632	13.225	125.3	CP2	2,4
J072040.31-000827.5	88814064	GSC 04816-00856	07 20 40.308	-00 08 27.521	13.135	62.0	CP2	2,4
J214528.67+423410.2	172212022	GSC 03192-01238	21 45 28.674	+42 34 10.256	11.888	75.4	CP2	
J231412.30+232336.9	57503106	GSC 02236-01035	23 14 12.305	+23 23 36.978	11.207	161.5	CP2	2,4
J012246.86+474343.9	82713145	GSC 03269-00936	01 22 46.858	+47 43 43.925	11.719	91.6	CP1	3,4
J022830.23+351753.0	294714195	HD 15282	02 28 30.440	+35 17 52.382	19.845	545.5	CP1	3,4
J023538.77+504829.1	206310079	GSC 03307-00765	02 35 38.776	+50 48 29.158	11.857	167.0	CP1	3,4
J024916.34+474840.8	172014239	GSC 03301-00058	02 49 16.344	+47 48 40.875	12.288	98.0	CP1	3,4
J033121.96+453110.7	408704129	GSC 03312-00096	03 31 21.960	+45 31 10.795	11.504	136.4	CP1	3,4
J035817.16+353234.0	181913164	GSC 02365-00334	03 58 17.157	+35 32 34.115	12.885	100.7	CP1	3,4
J041423.04+510959.8	379014063	GSC 03340-01232	04 14 23.039	+51 09 59.815	12.021	146.4	CP1	3,4
J042256.78+441458.8	190312238	GSC 02891-02087	04 22 56.780	+44 14 58.944	11.982	157.8	CP1	3,4
J051609.42+503544.8	168508158	HD 233093	05 16 09.425	+50 35 44.749	9.570	325.3	CP1	3,4
J051716.27+320140.4	89405073	GSC 02394-01286	05 17 16.275	+32 01 40.532	12.720	108.7	CP1	3,4
J052654.71-051454.6	181204075	GSC 04761-00694	05 26 54.707	-05 14 54.688	11.790	334.8	CP1	4
J053442.48+050744.1	307004089	GSC 00122-00503	05 34 42.490	+05 07 44.114	11.704	125.6	CP1	3,4
J053852.99+500732.1	191011033	GSC 03368-00681	05 38 53.025	+50 07 32.150	11.265	82.0	CP1	3,4
J055621.82+215854.1	116301217	GSC 01324-02312	05 56 21.833	+21 58 54.152	11.796	142.0	CP1	3,4
J055658.80+305431.7	127711190	GSC 02406-01503	05 56 58.805	+30 54 31.692	11.420	116.4	CP1	1,3,4
J061118.40+513036.5	380005061	GSC 03387-00370	06 11 18.406	+51 30 36.523	11.905	289.7	CP1	3,4
J061743.05+595315.3	169614033	GSC 03776-00815	06 17 43.066	+59 53 15.312	11.316	148.5	CP1	3
J063358.86+162851.1	43802152	GSC 01329-00314	06 33 58.866	+16 28 51.167	11.133	106.7	CP1	3,4
J063844.04+273220.6	189513009	UCAC4 588-03330	06 38 44.056	+27 32 20.719	14.855	60.8	CP1	3,4
J064705.49+263321.7	100205069	GSC 01901-00721	06 47 05.498	+26 33 21.676	11.683	77.0	CP1	3,4
J065620.88+234100.2	108810223	GSC 01894-00419	06 56 20.880	+23 41 00.159	12.613	122.6	CP1	3,4
J065626.12+053853.9	368911033	GSC 00161-00337	06 56 26.129	+05 38 53.960	12.573	104.5	CP1	3,4
J070252.43+211100.1	174915183	UCAC4 556-037142	07 02 52.425	+21 11 00.135	15.520	56.4	CP1	3
J072913.48+242111.9	140416192	GSC 01910-00845	07 29 13.479	+24 21 11.988	12.082	112.7	CP1	3,4
J082647.44+161418.4	432714119	GSC 01379-00095	08 26 47.367	+16 14 18.445	10.884	254.7	CP1	3,4
J083432.30+013758.7	137215069	GSC 00210-00002	08 34 32.308	+01 37 58.699	9.404	386.8	CP1	3,4
J083947.05-072231.4	111104095	GSC 04875-00091	08 39 47.053	-07 22 31.590	10.513	108.9	CP1	3,4
J084251.20-015717.7	125411209	GSC 04867-01502	08 42 51.205	-01 57 17.861	10.952	68.8	CP1	3,4
J084436.87+320618.2	130208121	GSC 02484-00400	08 44 36.869	+32 06 18.265	14.909	37.5	CP1	3,4
J093730.37+321651.6	22615081	GSC 02501-00330	09 37 30.287	+32 16 51.008	11.196	432.2	CP1	3,4
J093920.09-055123.1	83503117	GSC 04900-00542	09 39 20.089	-05 51 23.115	13.117	51.5	CP1?	
J115927.56+022614.0	237705132	BD+03 2582	11 59 27.564	+02 26 14.098	11.045	124.9	CP1	1,3,4
J131759.16+170150.3	425015052	GSC 01451-00443	13 17 59.162	+17 01 50.379	12.247	175.4	CP1	3,4
J191403.99+511612.5	250014100	GSC 03554-00217	19 14 04.024	+51 16 12.338	11.664	183.3	CP1	3,4
J191519.54+434913.1	362008084	GSC 03133-02227	19 15 19.543	+43 49 13.107	11.478	447.6	CP1	3
J192615.25+422836.6	154008048	GSC 03142-00964	19 26 15.257	+42 28 36.717	12.267	140.5	CP1	3,4
J193201.84+392304.9	373105196	GSC 03139-00006	19 32 01.739	+39 23 05.786	9.904	292.6	CP1	3,4
J193724.78+454300.2	247715139	GSC 03556-01543	19 37 24.820	+45 43 00.865	12.754	147.3	CP1	3,4
J195842.74+403448.3	367806224	UCAC4 653-084816	19 58 42.740	+40 34 48.231	12.735	135.5	CP1	3,4
J211930.96+244342.2	258415189	GSC 02190-02112	21 19 30.969	+24 43 42.321	11.864	150.0	CP1	3,4
J213435.04+410543.0	172204169	GSC 03187-00774	21 34 35.005	+41 05 43.022	10.933	330.8	CP1	3,4
J224509.70+081116.1	78213142	GSC 01152-01029	22 45 09.701	+08 11 16.000	14.255	92.2	CP1	3,4
J225451.47+514110.6	361915072	GSC 03634-01072	22 54 51.473	+51 41 10.686	11.895	294.0	CP1	3,4
J004534.75+452026.3	186715166	GSC 03262-00282	00 45 34.766	+45 20 25.352	12.471	172.6	comp?	4
J050321.41+512856.5	168514062	GSC 03356-00169	05 03 21.421	+51 28 56.567	10.754	229.6	comp?	
J125004.42+550602.1	152807229	GSC 03845-00640	12 50 04.514	+55 06 01.635	12.665	116.3	comp?	

References:

- 1 Renson & Manfroid (2009) 2 Hümmerich et al. (2020) 3 Qin et al. (2019) 4 Shang et al. (2022) 5 Scholz et al. (2019)

Table 8. Variability analysis results. Stars are sorted by increasing right ascension. The columns denote: (1) LAMOST identifier. (2) Alternative identifier. (3) Right ascension (J2000; GAIA EDR3). (4) Declination (J2000; GAIA EDR3). (5) VSX identifier. (6) VSX variability type. (7) VSX period (d). (8) TESS identifier. (9) Variability type deduced from analysis of TESS data. Types are explained in the remarks below the table. (10) Period (d) derived from TESS data.

(1) ID_LAMOST	(2) ID_alt	(3) RA(J2000)	(4) Dec(J2000)	(5) ID_VSX	(6) Type_VSX	(7) P_{VSX}	(8) ID_TIC	(9) Type_TESS	(10) P_{TESS}
J002559.10+555631.3	GSC 03657-00187	00 25 59.097	+55 56 31.114				449983408	const?	
J003933.02+273029.5	GSC 01744-02329	00 39 33.025	+27 30 29.417	V0496 And	EA	4.40262	25756249	EA	4.40869
J004127.44+220716.9	GSC 01193-00234	00 41 27.442	+22 07 16.944				434216252	eclipsor	5.7012
J020138.33+561624.4	UCAC4 732-01949	02 01 38.341	+56 16 24.493				445557996		
J020207.64+543927.9	GSC 03689-00919	02 02 07.642	+54 39 28.010				374568473	const?	
J020820.76+562433.0	HD 12921	02 08 20.633	+56 24 35.290						
J030240.87+522334.6	GSC 03322-00936	03 02 40.875	+52 23 34.692				116411454	ELL	1.04484
J031003.35+551804.4	HD 232754	03 10 03.359	+55 18 01.367						
J031638.78+494256.2	GSC 03319-00602	03 16 38.777	+49 42 55.989				117621124	const	
J031841.75+462842.1	GSC 03311-01885	03 18 41.776	+46 28 40.974				192843390	irr	
J031909.14+192811.7	BD+18 457	03 19 08.931	+19 28 11.753						
J032704.99+434028.5	GSC 02873-01933	03 27 04.997	+43 40 28.556				456144376	eclipsor	6.2902
J033909.14+523714.5	GSC 03716-00037	03 39 09.142	+52 37 14.550				428250707	const	
J034636.05+441159.3	GSC 02875-01237	03 46 36.054	+44 11 59.403				431964351	ELL	0.43026
J035000.80+580406.0	GSC 03725-01226	03 50 00.807	+58 04 06.118				86661062	const?	
J035033.65+525943.2	GSC 03717-00421	03 50 33.658	+52 59 43.279				449966196	const?	
J035205.73+351059.1	GSC 02364-02043	03 52 05.733	+35 10 59.126				94278532		
J040713.90+291832.1	GSC 01826-00710	04 07 13.878	+29 18 32.426	IL Tau	EA/SD	5.36062	348952490		
J041308.41+534045.9	GSC 03718-00545	04 13 08.415	+53 40 45.956				267695404	const?	
J041638.47+530600.9	GSC 03719-00690	04 16 38.473	+53 06 00.846				104848807	EW?	1.02151
J043336.04+451232.6	GSC 03342-00138	04 33 36.042	+45 12 32.709				28752151	ELL	1.08241
J043415.66+405139.5	UCAC4 655-022462	04 34 15.666	+40 51 39.552				155600657		
J043948.40+474848.5	GSC 03346-00854	04 39 48.401	+47 48 48.587				348102309	const?	
J044307.81+571907.8	GSC 03741-00200	04 43 07.813	+57 19 07.806	Mis V1381	EA	4.65	9953640	EA	4.64024
J050435.48+402559.7	UCAC4 653-028138	05 04 35.489	+40 25 59.682				122098910		
J050556.74+430528.8	GSC 02903-00983	05 05 56.760	+43 05 28.871				261149041	const?	
J051428.45+274324.3	GSC 01854-00033	05 14 28.465	+27 43 24.555	AS Tau	EA/SD	3.483328	61770518		
J053235.07+495218.6	GSC 03367-01174	05 32 35.073	+49 52 18.684				310350759	const	
J053414.62+215213.6	GSC 01309-01353	05 34 14.626	+21 52 13.641				437804190		
J053918.09+361716.2	GSC 02416-00657	05 39 18.088	+36 17 16.214	ASASSN-V J053918.09+361716.3	VAR	0	239106869		
J054113.82+351910.7	GSC 02412-01090	05 41 13.827	+35 19 10.725				116394274	puls?	0.36919
J054239.89+174652.7	HD 246608	05 42 39.841	+17 46 53.528				247473690		
J054329.26+000458.8	HD 290828	05 43 29.252	+00 04 58.970	GT Ori	UXOR	0	199955590	irr	
J054358.96+491845.6	GSC 03368-01318	05 43 58.958	+49 18 45.706				311231207	puls?	1.15559
J054834.63+234141.4	BD+23 1058	05 48 34.637	+23 41 41.489				358224196		
J055140.83-414108.5	GSC 09290-02782	05 51 40.835	+41 41 08.500				266348210	DSCT	0.15266
J055340.45+332003.9	UCAC4 617-029482	05 53 40.456	+33 20 03.995				312221983		
J055441.84+223317.7	GSC 01863-02412	05 54 41.850	+22 33 17.763	NSV 2719	0	0	118897886		
J055907.94-060737.6	GSC 04781-00953	05 59 07.949	-06 07 37.675				67279509	ELL	6.9642
J060706.46+245547.1	UCAC4 575-024208	06 07 06.470	+24 55 47.138				81186298		
J061810.01+411332.0	GSC 02930-00867	06 18 10.012	+41 13 32.113				258356786		
J062416.04+422125.4	GSC 02935-01774	06 24 16.047	+42 21 25.477				189945062	EA	10.687
J062618.73+174526.9	HD 257117	06 26 18.745	+17 45 27.254				438232591		
J062724.55+234931.0	UCAC4 570-028755	06 27 24.551	+23 49 31.048	HU Gem	EA	4.206669	426585626		
J064142.55+031421.9	GSC 00151-01200	06 41 42.552	+03 14 21.954				301494903	const?	
J064230.24+092626.7	HD 262371	06 42 30.247	+09 26 26.726				231162744	const	
J064751.97+522321.9	GSC 03402-01356	06 47 51.974	+52 23 21.876				453343612	eclipsor	1.42251
J065136.11+125351.1	HD 265136	06 51 36.153	+12 53 51.562				155306152	const	
J065141.20+070357.7	HD 265284	06 51 41.202	+07 03 57.750				235258580	const?	
J065300.06+010730.6	GSC 00149-01072	06 53 00.062	+01 07 30.643				237564914	const?	
J065606.26+033757.5	GSC 00153-01723	06 56 06.264	+03 37 57.524				237736667	irr	
J070219.92+162845.4	GSC 01344-00359	07 02 19.921	+16 28 45.453				457088125		
J071200.59+241137.2	GSC 01896-00475	07 12 00.593	+24 11 37.376				101573787		
J071340.29+380623.9	HD 55200	07 13 40.582	+38 06 30.260						
J071630.57+053405.5	GSC 00172-00143	07 16 30.576	+05 34 05.521				284555430	const	
J072719.01+015251.6	GSC 00169-00831	07 27 19.013	+01 52 51.702				318579975	const	
J074455.91+042805.1	GSC 00187-01505	07 44 55.913	+04 28 05.207				266811412	EA	5.9205
J075535.94-033455.4	GSC 04837-02525	07 55 35.947	-03 34 55.562				123194618	EA	4.02277
J080809.68+052950.7	GSC 04855-02705	08 08 09.691	+05 29 50.777				88684812	ELL	1.48389
J081646.65+040220.3	GSC 04856-00003	08 16 46.658	-04 02 20.468				178544181		
J085216.65+090518.7	BD+9 2072	08 52 16.652	+09 05 18.779				459056359		
J090754.79+212319.3	GSC 01407-00362	09 07 54.796	+21 23 19.322				386890261		
J092110.64+283147.9	HD 80535	09 21 10.656	+28 31 48.053				149418554	EA	3.18875
J093958.52-005332.0	GSC 04894-02078	09 39 58.526	-00 53 31.465				62730967	ELL	1.35403
J180605.37+020543.8	GSC 00434-03484	18 06 05.379	+02 05 43.834				390639438		
J190401.96+415350.8	GSC 03128-02038	19 04 01.952	+41 53 50.944				120687891		
J195131.48+484558.9	GSC 03565-01258	19 51 31.489	+48 45 58.977				28308522	const?	
J200641.70+274307.0	GSC 02162-01397	20 06 41.705	+27 43 07.005				244659647	const?	
J213345.79+423744.6	GSC 03191-01168	21 33 45.789	+42 37 44.569				240465526	const?	
J213720.80+132827.0	BD+12 4653	21 37 20.905	+13 28 28.499	AQ Peg	EA/SD	5.5485028			
J225304.50+544503.0	GSC 03988-01889	22 53 04.500	+54 45 03.047				388968595	EA	1.02991
J225542.92+555816.9	GSC 03989-00149	22 55 42.921	+55 58 16.904				367689958	const	
J225954.10+421753.8	GSC 03223-03570	22 59 54.112	+42 17 53.841				154930789		
J231357.71+545812.0	GSC 04002-01262	23 13 57.525	+54 58 12.204				371823816	artefact?	
J232258.57+541829.2	GSC 03999-01276	23 22 58.579	+54 18 29.297				319506298	ELL	8.8806

Variability types in Column 9 are as follows:

const = constant; irr = irregular variability; puls = pulsational variability; eclipsor = eclipsing binary; EA = eclipsing binary of Algol-type; EW = eclipsing binary of W UMa-type; ELL = ellipsoidal variable; DSCT = delta Scuti star

ticular, the institutions participating in the *Gaia* Multilateral Agreement. This research has made use of the SIMBAD database, operated at CDS, Strasbourg, France.

REFERENCES

- Abt H. A., Moyd K. I., 1973, *ApJ*, **182**, 809
 Anusha R., et al., 2021, *MNRAS*, **501**, 5927
 Arenou F., et al., 2018, *A&A*, **616**, A17
 Baade D., et al., 2016, *A&A*, **588**, A56
 Bailer-Jones C. A. L., Rybizki J., Fouesneau M., Mantelet G., Andrae R., 2018, *AJ*, **156**, 58
 Bayo A., Rodrigo C., Barrado Y. Navascués D., Solano E., Gutiérrez R., Morales-Calderón M., Allard F., 2008, *A&A*, **492**, 277
 Bernhard K., Otero S., Hümmerich S., Kaltcheva N., Paunzen E., Bohlsen T., 2018, *MNRAS*, **479**, 2909
 Bessell M. S., Brett J. M., 1988, *PASP*, **100**, 1134
 Bohlender D., 2016, in Sigut T. A. A., Jones C. E., eds, Astronomical Society of the Pacific Conference Series Vol. 506, Bright Emissaries: Be Stars as Messengers of Star-Disk Physics. p. 275
 Bressan A., Marigo P., Girardi L., Salasnich B., Dal Cero C., Rubele S., Nanni A., 2012, *MNRAS*, **427**, 127
 Campante T. L., et al., 2016, *ApJ*, **830**, 138
 Chojnowski S. D., et al., 2015, *AJ*, **149**, 7
 Cui X.-Q., et al., 2012, Research in Astronomy and Astrophysics, **12**, 1197
 Eiroa C., et al., 2021, *A&A*, **653**, A115
 Ferlet R., Hobbs L. M., Vidal-Madjar A., 1987, *A&A*, **185**, 267
 Gaia Collaboration et al., 2016, *A&A*, **595**, A1
 Gaia Collaboration et al., 2018a, *A&A*, **616**, A1
 Gaia Collaboration et al., 2018b, *A&A*, **616**, A10
 Gray R. O., Corbally C. J., 2009, Stellar Spectral Classification
 Gray R. O., Corbally C. J., 2014, *AJ*, **147**, 80
 Gray R. O., Garrison R. F., 1987, *ApJS*, **65**, 581
 Gray R. O., et al., 2016, *AJ*, **151**, 13
 Green G. M., Schlafly E., Zucker C., Speagle J. S., Finkbeiner D., 2019, *ApJ*, **887**, 93
 Huang C. X., et al., 2020a, *Research Notes of the American Astronomical Society*, **4**, 204
 Huang C. X., et al., 2020b, *Research Notes of the American Astronomical Society*, **4**, 206
 Hümmerich S., et al., 2018, *A&A*, **619**, A98
 Hümmerich S., Paunzen E., Bernhard K., 2020, *A&A*, **640**, A40
 Jaschek M., Slettebak A., Jaschek C., 1981, Be Star Newsletter, **4**, 9
 Jaschek M., Jaschek C., Egret D., 1986, *A&A*, **158**, 325
 Jaschek M., Jaschek C., Andrillat Y., 1988, *A&AS*, **72**, 505
 Kunimoto M., et al., 2021, *Research Notes of the American Astronomical Society*, **5**, 234
 Labadie-Bartz J., et al., 2017, *AJ*, **153**, 252
 Labadie-Bartz J., et al., 2018, *AJ*, **155**, 53
 Labadie-Bartz J., Carciofi A. C., Henrique de Amorim T., Rubio A., Luiz Figueiredo A., Ticiani dos Santos P., Thomson-Paressant K., 2022, *AJ*, **163**, 226
 Li G.-W., et al., 2018, *ApJ*, **863**, 70
 Luo A. L., Zhao Y. H., Zhao G., et al. 2018, VizieR Online Data Catalog, **5153**, 0
 Meeus G., Waelkens C., Malfait K., 1998, *A&A*, **329**, 131
 Miroshnichenko A. S., Bergner Y. K., Kuratov K. S., Mukhanov D. B., Sheikina T. A., 1996, *Astronomy Reports*, **40**, 509
 Negueruela I., 2004, *Astronomische Nachrichten*, **325**, 380
 Paunzen E., 2015, *A&A*, **580**, A23
 Paunzen E., Vanmunster T., 2016, *Astronomische Nachrichten*, **337**, 239
 Paunzen E., Hümmerich S., Bernhard K., 2021, *A&A*, **645**, A34
 Porter J. M., Rivinius T., 2003, *PASP*, **115**, 1153
 Qin L., et al., 2019, *ApJS*, **242**, 13
 Renson P., Manfroid J., 2009, *A&A*, **498**, 961
 Ricker G. R., et al., 2014, *Transiting Exoplanet Survey Satellite (TESS)*. p. 914320, doi:10.1111/12.2063489
 Ricker G. R., et al., 2015, *Journal of Astronomical Telescopes, Instruments, and Systems*, **1**, 014003
 Rivinius T., Štefl S., Baade D., 2006, *A&A*, **459**, 137
 Rivinius T., Carciofi A. C., Martayan C., 2013, *A&ARv*, **21**, 69
 Scholz R. D., Chojnowski S. D., Hubrig S., 2019, *A&A*, **628**, A81
 Shang L.-H., et al., 2022, *ApJS*, **259**, 63
 Shridharan B., Mathew B., Nidhi S., Anusha R., Arun R., Kartha S. S., Kumar Y. B., 2021, *Research in Astronomy and Astrophysics*, **21**, 288
 Skrutskie M. F., et al., 2006, *AJ*, **131**, 1163
 Slettebak A., 1982, *ApJS*, **50**, 55
 Underhill A., Doazan V., 1982, B stars with and without emission lines, parts 1 and 2; Monograph Series on Nonthermal Phenomena in Stellar Atmospheres - NASA SP 456. Paris: Center National de la Recherche Scientifique (CNRS) and Washington: NASA
 Vioque M., Oudmaijer R. D., Schreiner M., Mendigutía I., Baines D., Mowlavi N., Pérez-Martínez R., 2020, *A&A*, **638**, A21
 Waters C. Z., Hollek J. K., 2013, *PASP*, **125**, 1164
 Watson C. L., Henden A. A., Price A., 2006, Society for Astronomical Sciences Annual Symposium, **25**, 47
 Yuan H. B., Liu X. W., Xiang M. S., 2013, *MNRAS*, **430**, 2188
 Zavada P., Příška K., 2022, *AJ*, **163**, 33
 Zhang Y.-J., et al., 2022, *ApJS*, **259**, 38
 Zhao G., Zhao Y.-H., Chu Y.-Q., Jing Y.-P., Deng L.-C., 2012, *Research in Astronomy and Astrophysics*, **12**, 723

APPENDIX A: TESS LIGHT CURVES

This section contains the TESS JD light curves of the final sample of shell stars (cf. Section 3.4).

This paper has been typeset from a $\text{\TeX}/\text{\LaTeX}$ file prepared by the author.

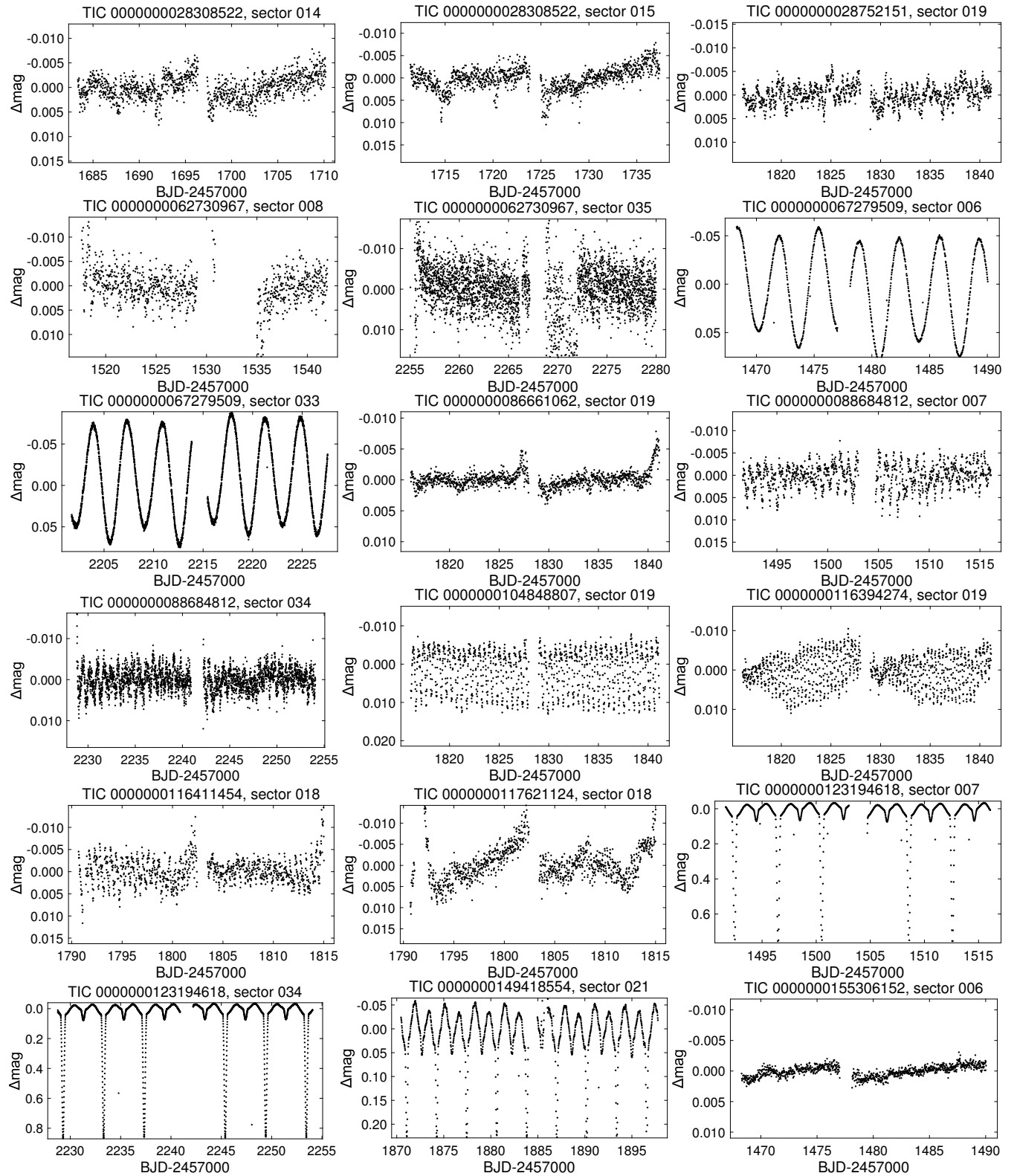
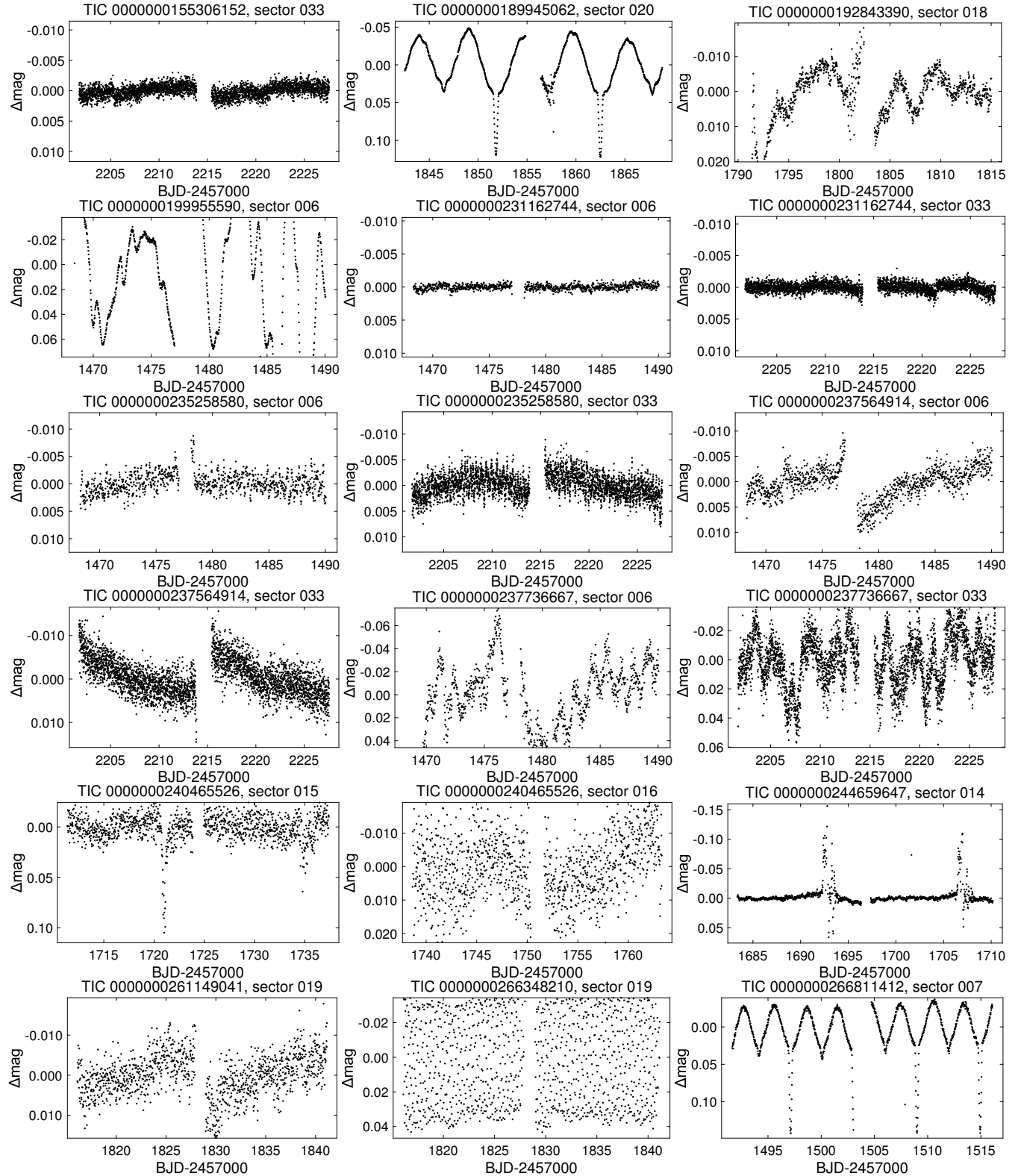


Figure A1. TESS light curves of all objects contained in the final shell star sample.

**Figure A2.** TESS light curves of all objects contained in the final shell star sample.

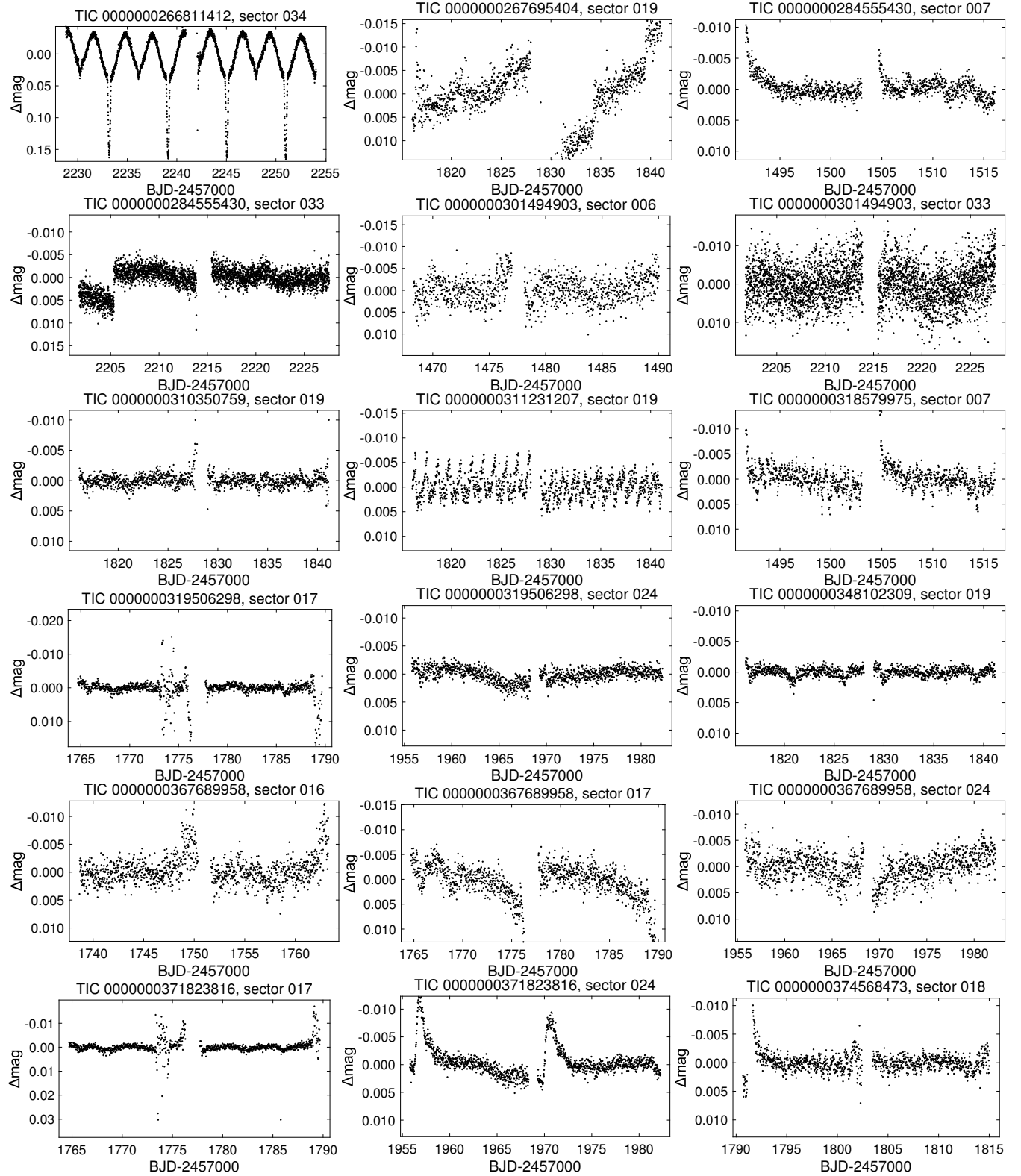
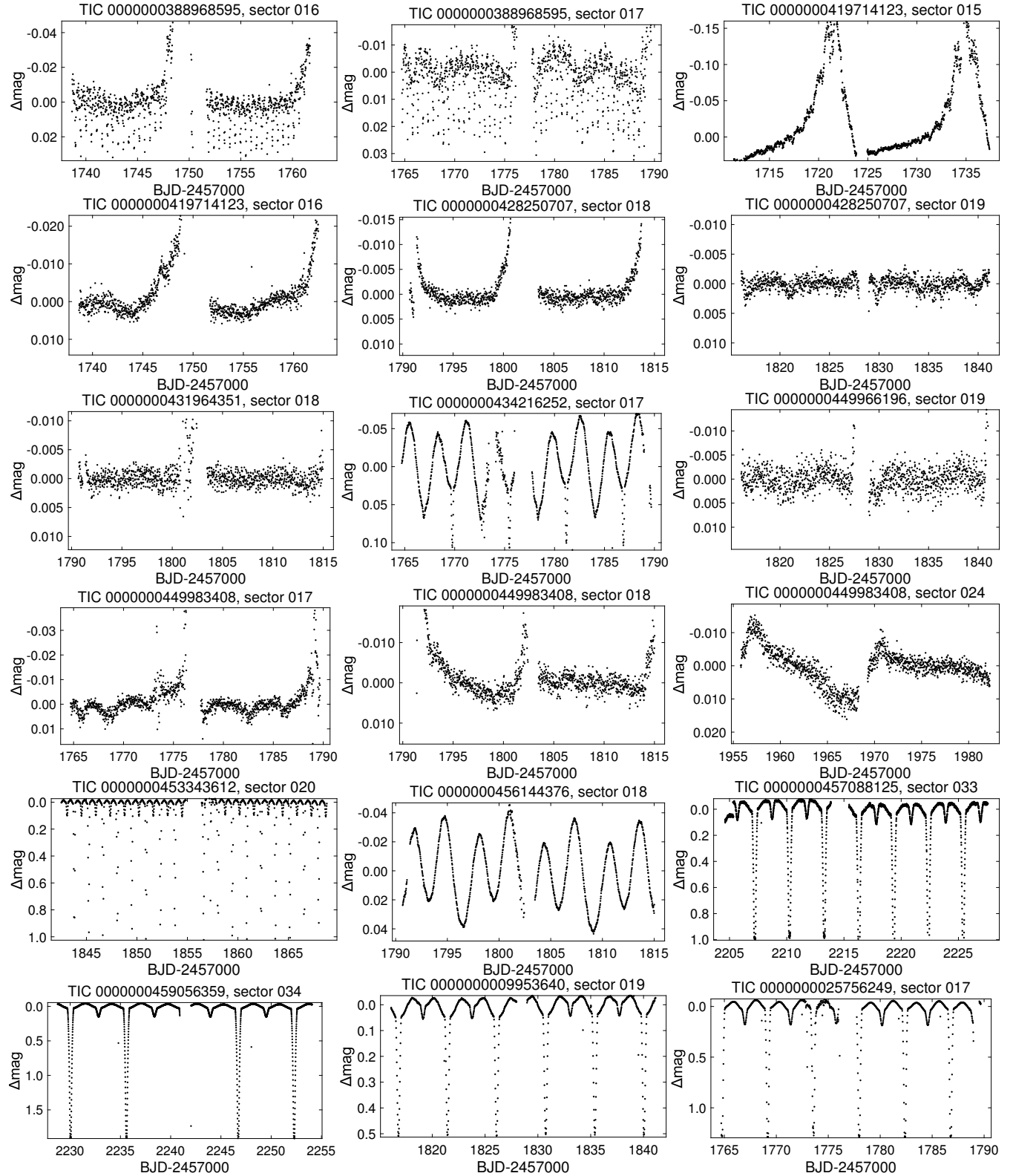


Figure A3. TESS light curves of all objects contained in the final shell star sample.

**Figure A4.** TESS light curves of all objects contained in the final shell star sample.